2018-01-01

Extraction Of Fiber Morphology From Sem Images For Quality Control Of Fiber Reinforced Composites Manufacturing

Md Fashiar Rahman
University of Texas at El Paso, mrahman13@miners.utep.edu

EXTRACTION OF FIBER MORPHOLOGY FROM SEM IMAGES FOR QUALITY CONTROL OF FIBER REINFORCED COMPOSITES MANUFACTURING

MD FASHIAR RAHMAN

Master's Program in Computational Science Program

APPROVED:

Tzu-Liang (Bill) Tseng, Ph.D., Chair

Jianguo Wu, Ph.D., Co-Chair

Yirong Lin, Ph.D.

M Shahriar Hossian, Ph.D.

Charles Ambler, Ph.D.
Dean of the Graduate School

EXTRACTION OF FIBER MORPHOLOGY FROM SEM IMAGES FOR QUALITY CONTROL OF FIBER REINFORCED COMPOSITES MANUFACTURING

by

MD FASHIAR RAHMAN, BSc in IPE

THESIS

Presented to the Faculty of the Graduate School of

The University of Texas at El Paso

in Partial Fulfillment

of the Requirements

for the Degree of

MASTER OF SCIENCE

Computational Science Program

THE UNIVERSITY OF TEXAS AT EL PASO

December 2018

Acknowledgements

I would first like to express my sincere gratitude to my research advisor Dr. Tzu-Liang (Bill) Tseng and academic advisor Dr. Ming-Ying Leung who gave me continuous support of my UTEP life. Their guidance helped me in all the time to continue my academic activities alongside my research and writing of this thesis. I could not have imagined to fulfill my objectives without having their support.

Besides my advisor, I would like to thank my thesis committee co-chair Dr. Jianguo Wu. I feel lucky to be supervised by such an excellent and enthusiastic expert in my field of research. I found him available whenever I face and trouble or had a question about my research. He consistently steered me in the right direction and innovative suggestion.

In addition, I would be grateful to my thesis committee Dr. Yirong Lin, Dr. Mahmud Shahriar Hossain for serving on my committee and providing helpful suggestion to improve my thesis.

My sincere thanks also goes to my fellow labmates and the CQPSI research group Dr. Hoejin Kim, Dr. Carlos A Garcia Rosales, Dr. Ivan A Renteria, Anabel Renteria Marquez, Yuxin Wen and Hoglun Xu, who provided me an intensive support and accompany in my studies. Without they precious support it would not be possible to conduct this research.

Last but not the least, I'm blessed and I thank God for every day for everything that happens to me. I must express my very profound gratitude to my parents and to my wife for providing me with unfailing support and continuous encouragement throughout my years of study and accomplishing my goals.

Abstract

The morphology of fibers (e.g. spatial uniformity, orientation, and length) plays a decisive role in determining the material properties or fabrication quality of fiber-reinforced nanocomposites. Hence, determining the morphology becomes a very critical issue in the field of nanocomposite quality control. The conventional way of quality inspection is to take the scanning electron microscopic (SEM) images of the cross-section of composite material and do the visual checking of these SEM images to evaluate the nanofiber alignment and length distribution. But this type of inspection is often subjective, inaccurate and time consuming. Moreover, the extremely small size of nanofibers makes the quality control evaluation process very tedious. This research attempts to fill this gap and presents an image based automatic method to leverage the morphology analysis of fibers embedded into the hosting material. The proposed method consists of two broad steps, namely fiber segmentation and quantitative analysis of segmented fibers. One particular challenge in fiber segmentation step is to segment the overlapped fibers from the SEM image, especially in a very high density fiber environment. To handle this issue, we develop four methods, namely, the simple Hough Transform, partitioning Hough Transform, gradient based Hough Transform, and density based clustering (DBSCAN) approach, to automatically identify the fibers from the SEM images. In the second step we extract the fiber morphology based on the segmented fibers and perform the quantitative analysis. We compare the fiber extraction result among the methods. The methods can extract up to 97% fibers from the SEM image in the very high fiber density environment, which expedite to acquire a reliable characterization of fiber morphology. The performance of these methods are thoroughly evaluated and compared through simulation studies and real case studies.

Table of Contents

List of Tables

List of Figures

Chapter 1: Introduction

1.1 Introduction

Nanomaterials are increasingly becoming part of our daily lives. Their novel properties, that are not apparent in larger forms of the same material, has led to their desirability and exploration in a wide range of applications. Nanomaterials can be defined as substances that are intentionally produced, manufactured or engineered to have specific properties and one or more dimensions typically between 1 and 100 nanometers. Scientists found that when the diameters of polymer fibers materials are shrunk from micrometers to submicron or nanometers, some amazing characteristics would appear. These characteristics include high strength, high stiffness and light weight, and many other functional properties, such as high energy density in capacitors [1]. Because of these unique properties resulting in improved performance of final products, nanomaterials are widely used in numerous end-user industries. As a result the nanomaterial market is increasing rapidly over the year [2]. Figure 1.1 shows the growth of Nano-material market in terms of revenue (USD Billion).

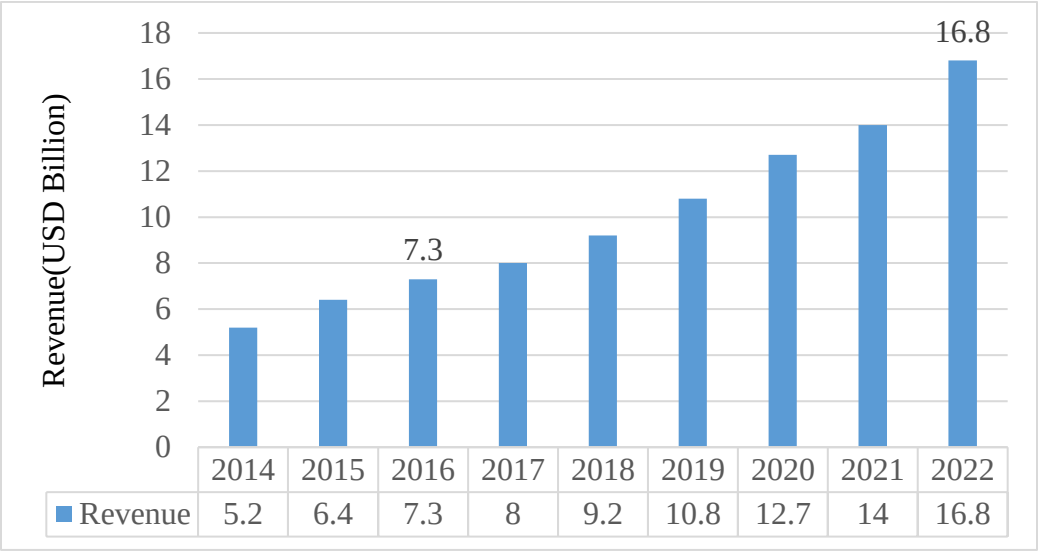

Figure 1.1: Global Nano-material market

Markets nanomaterials are currently impacting include healthcare, sporting goods, personal care, food and beverage, home and garden, automotive, aerospace, consumer electronics and computing etc. The key vendors of nanomaterials market are focusing aggressively in innovation, as well as on including advanced technologies in their existing products. Recently, nanocomposites with high energy densities have received a great interest for use in advanced electronic devices and electric power systems since they can be designed to offer a combination of both high dielectric permittivity and dielectric strength [3]. With the help of nanotechnology, new nanofiber material piezoelectric material provide the ability to bend and stretch also they are attractive for pressure sensors and mechanical energy harvests [4].

1.2 Background and Literature Review

Fibers are noble reinforcements to increase the mechanical properties of composites materials. The dispersion and alignment of fibers in the base material play a decisive role in determining the final properties of composites. The composite material is often stronger along the orientation of the fiber and weaker in a direction perpendicular to the fiber orientation [5]. In structural application uniform distribution of nanofibers in terms of both spatial location and orientation may be desirable to achieve the best mechanical properties. However, in some other applications, well-aligned fibers may be more preferable. Recently research shows that well-aligned fillers can significantly enhance the dielectric properties of the base material, specifically the dielectric permittivity and breakdown strength [6, 7]. Bown et al. created anisotropic filler for composites by using a dielectrophoretical assembly process. It was found that the sample with aligned filler had a dielectric constant approximately three times higher than that with random filler [8]. In the dielectric nanocomposites manufacturing used in high performance capacitors, well-aligned nanofibers could increase both permittivity and breakdown strength, and therefore increase the energy density of capacitors [9]. These results indicate that the orientation of the filler of nanocomposites must be carefully controlled and inspected to obtain the desired performance.

Factors like fiber location, size distribution, and orientation distribution are needed to get an authentic quality evaluation. The conventional approach of morphology analysis involves the visual inspection of microscopic images after taking the cross-section of the composite materials, which is time consuming and subjective. However, it is unrealistic to collect all these information manually. Therefore, an automatic quantitative analysis method is highly desirable for quality assessment. Therefore, automatic fiber extraction from SEM images is highly desirable for quality assessment.

The scanning electron microscope (SEM) uses a focused beam of high-energy electrons to generate a variety of signals at the surface of solid specimens [10]. The signals that derive from electron-sample interactions reveal information about the sample including morphology (texture), chemical composition, crystalline structure and orientation of materials making up the sample. In most applications, data are collected over a selected area of the surface of the sample and a 2-dimensional image is generated that displays the fibers in the form of the tiny line (rectangular shape). In the first step of morphology analysis, we need to segment these tiny lines from the SEM images. Image processing techniques have been successfully used for the morphology analysis of nanoparticles (circular and elliptical shape) both in biomedical and material science field. For example, ImageJ, a popular freeware tool provided by NIH, is used for the extraction and quantification of fluorescence particles [11] in biomedical field. Machine learning approach has also been introduced to locate the particle's position in the images based on Haar features [12]. Ellipse fitting techniques and watershed algorithm are used to separate the uniformly shaped particles from the background [13, 14]. The particle overlapping phenomenon is also well tackled in the literature of nanoparticle field [15]. However, there are very limited automated fiber (axial particulates) segmentation and methodologies in the existing methodologies. The Hough Transform (HT) can be used in detecting line [16], but a bottleneck is the decreasing efficiency of fibers segmentation when the fiber density increases in the hosting material. Kimura et al. [17] proposed an algorithm to measure the root length through image processing. Kawabata et al. [18] developed an image processing technique to detect and count asbestos fibers. Autocorrelation

functions (ACFs) provide a measure of pattern analysis for qualitative assessment [19]. The ridge detection techniques integrating with textons enable the ACFs to facilitate the quantitative analysis of aligned nanowires based on images [20]. However all these method is ineffective to segment fibers from SEM images of composites materials because of the phenomenon called fiber overlapping and consequently the reliable extraction of morphology analysis got hampered.

Our objective in this paper is to develop an effective and automated procedure that can attain a much higher segmentation rate of fibers from SEM images. By accomplishing higher segmentation, we can extract statistically more reliable distribution for orientations and sizes of fibers. The principle hindrance behind achieving the higher segmentation rate is the fiber overlapping phenomenon. To tackle this issue, we developed four methods to investigate how these methods performs with the overlapping phenomenon. In the first method we use the Hough Transform method following some basic image processing operations like dilation, erosion, Skeletonization etc. In the second method, we first partition the fiber with connected component and then apply the Hough Transform. In the third method, the gradient based Hough Transform is used to segment the fibers. We introduce a more innovative approach in the fourth method. The basic strategy in this method is to clustering the line pixels and crossing pixels. Later we remove the crossing pixels and merge the line pixels based on their continuity and orientations. Image processing techniques integrating the density-based clustering (DBSCAN) algorithm are deployed for this purpose. Following the fiber segmentation, we extract the orientation and length distribution using the spatial location of fibers. Subsequently, the extracted result has been validated through statistical analysis. The method was evaluated using artificially generated images. A comparison with experimental images was also entailed in this paper.

The rest of the thesis is organized as follows. In chapter 2, we developed four methods based on opening operation and Hough Transform to segment the Nano-fibers. The methodologies and algorithms are introduced in this chapter. The four methods are thoroughly investigated with artificially generated SEM images and two real images. A comparison of fiber segmentation result among the four methods is also shown in this chapter. Chapter 3 represents another fiber

segmentation techniques based density based clustering algorithm to expedite the morphology analysis (orientation and length distribution) of fibers. Six different set orientation is used to simulate the image and the empirical distribution is compared with the true distribution. The two real image mentioned in chapter 2 are also used in this chapter to demonstrate the real case study. This chapter also entails the Kolmogorov-Smirnov (K-S) test to show the confident of extracted distribution. Chapter 4 summarizes the work to date and introduce the future work.

Chapter 2: Fiber Segmentation

Segmentation subdivides an image into its constituent regions or object. The success of subdivision depends on mining the details information of segmented part of the image. This means segmentation should be stopped once we get the interest of our application. In SEM image, as the shape of a fiber is pretty much likely to be a line, it is considered that each line indicates a fiber in the image of composites. In this section, four methods will be introduced to extract the nanofibers (lines) from the SEM image.

2.1 Opening Method Based Fiber Detection

In this subsection, a method for detecting fiber has been proposed based on the "Opening" [21] operator. The opening of image A by a structuring element (SE) B is denoted (AoB) and is defined as

$$AoB = (A \ominus B) \oplus B \tag{1}$$

Where, $\ominus$ and $\oplus$ denote the "erosion" and "dilation" operation, respectively. Dilation is the morphologic transformation which combines two sets using vector addition of set elements. If A and B are the subset of N-space, the dilation of A by B is denoted by A$\oplus$B and is defined as

$$A \oplus B = \{c \in E \mid c = a + b \text{ for some } a \in A \text{ and } b \in B\} \tag{2}$$

Conversely, erosion is the morphological transformation which combines two sets using the vector subtraction of set elements. The erosion of A by B is defined by

$$A \ominus B = \{x \in E \mid x + b \in E \text{ for every } b \in B\} \tag{3}$$

In opening method, the structuring element B acts as a probe which moves across the image A and removes the objects that are smaller than SE using erosion operation. Later dilation operation is employed to restores the shape of the reaming objects. However, restoring accuracy highly depends on the type of structuring element and the shape of restoring objects. In this proposed method, we took the line structuring element with certain length. The SE is varied with all possible angles ranging from -89 to 90 and moved over the SEM image to open the nanofibers.

Consequently, the nanofibers which are less than the SE are opened. Since the nanofibers are rectangular in shape and are often larger than the SE, a single fiber may be detected multiple times by different SE's with close orientations. As illustrated in Figure 1(a), each fiber has been detected multiple times (marked by boundaries of different colors). Hence we need to merge these fibers or remove the duplicated segmentation. It is obvious that, if a fiber is opened multiple times, their centroids and the orientations will be very close. Based on this fact, we can check the closeness of the opened fibers and keep the desired one. The procedure is depicted in Figure 2.1 and the algorithm is illustrated in Table 2.1.

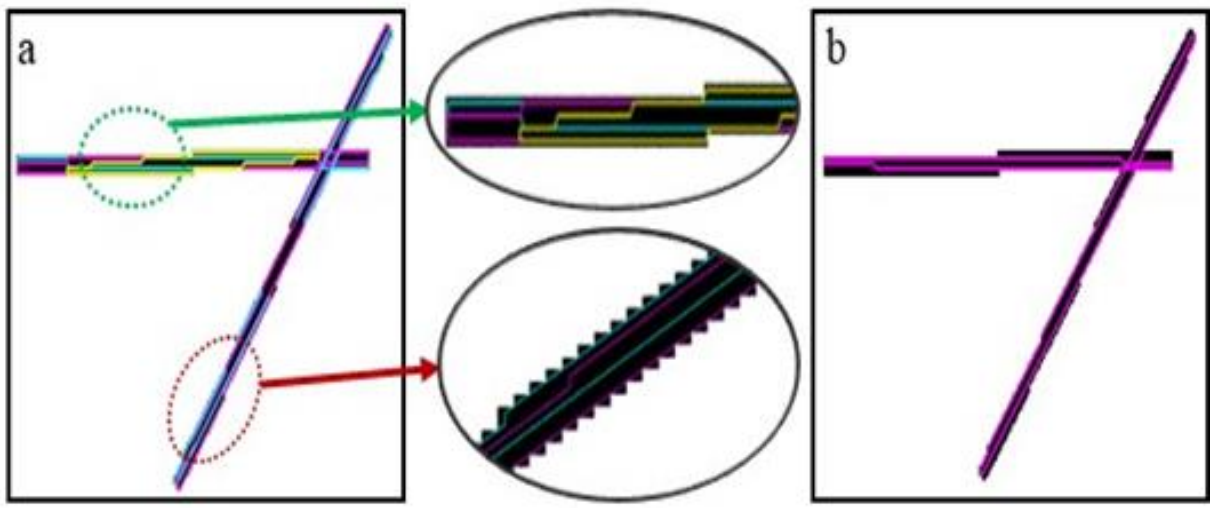

Figure 2.1: Opening method based fiber detection procedure, (a) detected boundaries after opening operation with duplicated detection (b) duplication deletion

Table 2.1: Opening method based nanofiber extraction algorithm

1. Convert the SEM image into binary image
2. For different angle θ ranging from -89 to 90

a) Perform “Opening” operation on binary image with line structure element with angle θ
b) Find out the boundary of each opened image
c) Extract the centroid and orientation of each opened image

3. End
4. For all of the orientation
    a) Check the closeness of each pair of detected fibers based on their centroid and orientations
    b) If closeness of the fibers is below a certain threshold
        i. Treat them as a single fiber.
5. end

2.2 Simple Hough Transform Based Fiber Detection

Hough Transform is a mapping of a line from the spatial domain to another parameter space. It was first introduced by Paul Hough in 1962 [22]. Later it was extended to identify the arbitrary shapes, e.g., circles and ellipse, and it was named “Generalized Hough Transform” [23]. In Hough Transform, a straight line is represented by the equation 4.

$$\rho = x\cos\theta + y\sin\theta \quad (4)$$

Where, ρ is the length of the normal vector from the origin to the straight line and θ is the angle it makes with the x axis. The ρ-θ parameter space is subdivided into small accumulator cells to form a two-dimensional matrix. The parameter θ and ρ are usually limited to $\pm\pi / 2$ and $\sqrt{M^2 + N^2}$ respectively, where (M, N) is the image size. Based on this parameterization each image point (x, y) generates a sinusoidal curves in (θ, ρ) space. The points, belongs to a particular line, map to the (θ, ρ)space and intersect at a unique accumulator cell. This accumulator cell identifies the value of ρ and θ for the corresponding line. Thus lines are determined by the intersection of many of these sinusoids. As illustrated in Figure 2.2, three points

$\{(49,1), (25,25), (1,49)\}$ generates three sinusoidal curves *a*, *b* and *c* respectively. Since, these three points belong to the same line, they intersect at a common point d, which gives the parameter of $\rho = 33.9$ and $\theta = 45$ for the corresponding line.

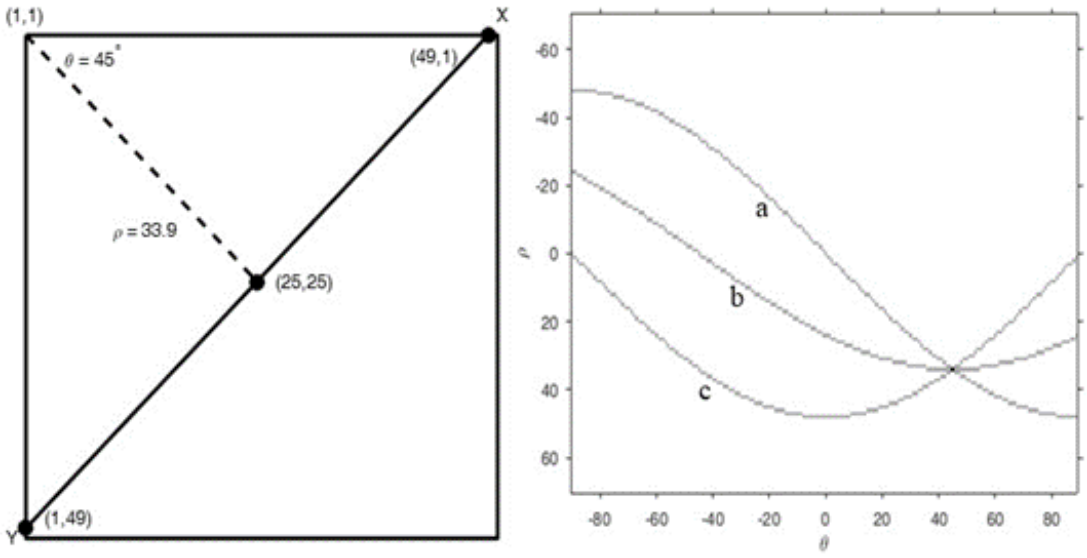

Figure 2.2: Illustration of Hough Transform

To extract the nanofibers, we could use Hough Transform to detect lines in SEM image. But the direct use of HT generates two major issues. The first issue is that if the fiber is large in width, multiple lines will be detected on the same fiber. Secondly, the accumulator cell can gather points which are in the same line but they are actually from different fibers. To address the first issue, "Skeleton" operation [24] could be used to get the skeletonized image. Given a set point set *A*, the skeleton operation $S(A)$ is defined as follows:

$$S(A) = \cup_{k=0}^{M} S_k(A) \tag{5}$$

$$S_k(A) = (A \ominus kB) - [(A \ominus kB)\ o\ B] \tag{6}$$

Where, M indicates the last iterative step before A erodes to an empty set which defined by equation 4 and *k* indicates how many times A is eroded ($\ominus$) with the structuring element *B* and (o) indicates the opening operation.

$$M = \max\{k|(A \ominus kB) \neq \emptyset\} \quad (7)$$

To overcome the second issue, the continuity of the points is evaluated by computing the distance of a pair of point. Then the gap is checked based on a threshold value. If the gap between two sets of point is bigger than the threshold, HT considers them as from separate lines; otherwise they are from the same line.

2.3 Partitioning Hough Transform

In Simple HT, "skeleton" operation is employed to alleviate the detection of multiple lines on a single fibers. However, there is still an issue in the above method. The skeleton of other fibers could contribute to the accumulator cell values and may significantly influence the detection accuracy, especially when the density of fiber is very large. To overcome this problem, we propose the partitioning Hough Transform, where the partitioning is first applied to segment SEM images into multiple images based on connected components and then apply Hough transform to each segmented image. The partitioning Hough Transform is illustrated in Table 2.2.

Table 2.2: Partitioning Hough Transform for nanofiber segmentation algorithm

1. Convert the SEM image into binary image
2. Partition the binary image into n SEM images with each having one connected component.
3. For $i = 1{:}\,n$
    a) Extract the morphological "skeleton" of image i
    b) Perform Hough Transform on image i to get the Hough matrix
    c) Identify the peaks of the Hough matrix
    d) Detect Hough line based on peaks and Hough matrix
4. End

2.4 Gradient based Hough Transfer

As the density of fibers increases, there would be more fibers crossed with each other. The fiber crossing will significantly influence the shape of the skeleton (from straight lines to curved lines) as shown in Figure 2.3. Therefore it would reduce the detection accuracy of the HT method.

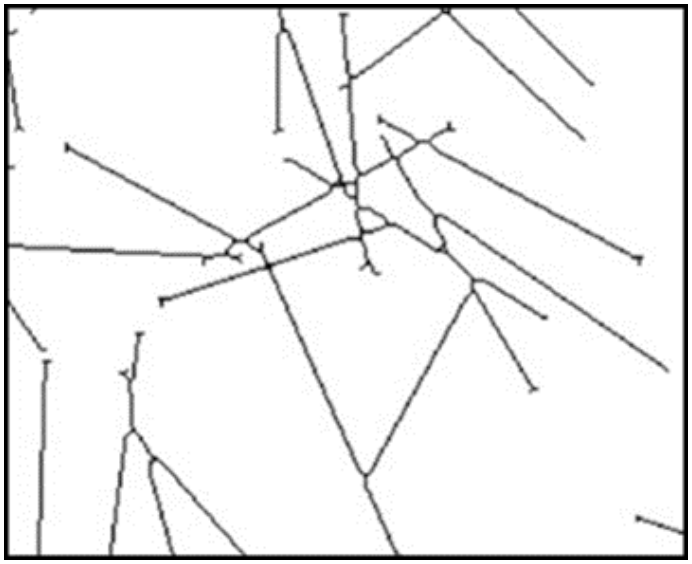

Figure 2.3: Skeleton of multiple crossed fiber

To solve this issue, another innovative and more effective method is proposed here. This method is the extension of the standard Hough Transform-where each pixel of the fiber boundaries is mapped to a single cell in the discretized (θ, ρ) space based on its gradient. The rational is that the gradient direction of the fiber boundary is approximately equal to the line orientation θ in Equation 4. Instead of mapping each pixel to a curve in (θ, ρ) space, we only increase the corresponding accumulator with θ equal to the gradient. Using this idea, we can reduce the number of useless votes.

Finding gradient orientation involves two major steps. The first step is to detect the boundary of all fibers and then to measure the changes in x and y coordinates along each boundary.

After extracting the gradient information- we can use the gradient based Hough Transform algorithm to detect the boundaries.

Boundaries can be easily extracted through various existing methods, such as "Freeman Chain Code" [25, 26], "Minimum-Perimeter Polygon (MPP)" [27, 28] and "Moore Boundary Tracing Algorithm" [29]. Let g_{x_i} and g_{y_i} be components of the gradient at (x_i, y_i). As the boundary data set (B) is a collection of sequential pairs of x and y coordinates along the boundary, we can easily measure the g_{x_i} and g_{y_i} by taking the difference between two points using equation 8.

$$B = \{(x_i, y_i)\}$$
$$\left(g_{x_i}, g_{y_i}\right) = (x_{i+l} - x_i, y_{i+l} - y_i) \quad (8)$$

Where, l is the step size. Then the gradient direction θ for pixel (x_i, y_i) can be calculated by equation 9.

$$\theta_i = \tan^{-1} \frac{g_{y_i}}{g_{x_i}} \quad (9)$$

After finding the gradient orientation, we use these information to detect the fibers using the gradient based Hough Transform. The algorithm is illustrated in Table 2.3.

Table 2.3: Gradient based Hough Transform for nanofiber segmentation algorithm

1. Convert the SEM image into binary image
2. Extract the boundaries of fibers
3. For each of the boundary pixel (x_i, y_i)
   a) Calculate the gradient θ_i
   b) Calculate the parameter $\rho_i = x_i cos\theta_i + y_i sin\theta_i$
   c) Increase the accumulator $A(\theta_i, \rho_i) = A(\theta_i, \rho_i) + 1$
4. End
5. Detect the peaks form the Hough matrix *A*
6. Find the ρ and θ for the corresponding peaks

7. Detect the fibers using corresponding ρ and θ

2.5 Simulation Study

In the following sections, simulated SEM images of fiber reinforced composites are used to evaluate the proposed methods. The image resolution is 2400×1800 pixels. The fibers are uniformly distributed with density$\rho = 0.0001$ fiber/pixel^2. The length of each fiber follows a normal distribution with mean of 120 pixels and standard deviation of 20 pixels. The width is fixed as $2\sigma = 4$ pixels. The intensity of the gray image at each pixel follows a truncated normal distribution within 0 to 255 with 192 ± 32 (mean ± deviation). The fiber orientation is uniformly distributed. Figure 2.4 shows four simulated SEM images with 50, 100, 200, 400 fibers.

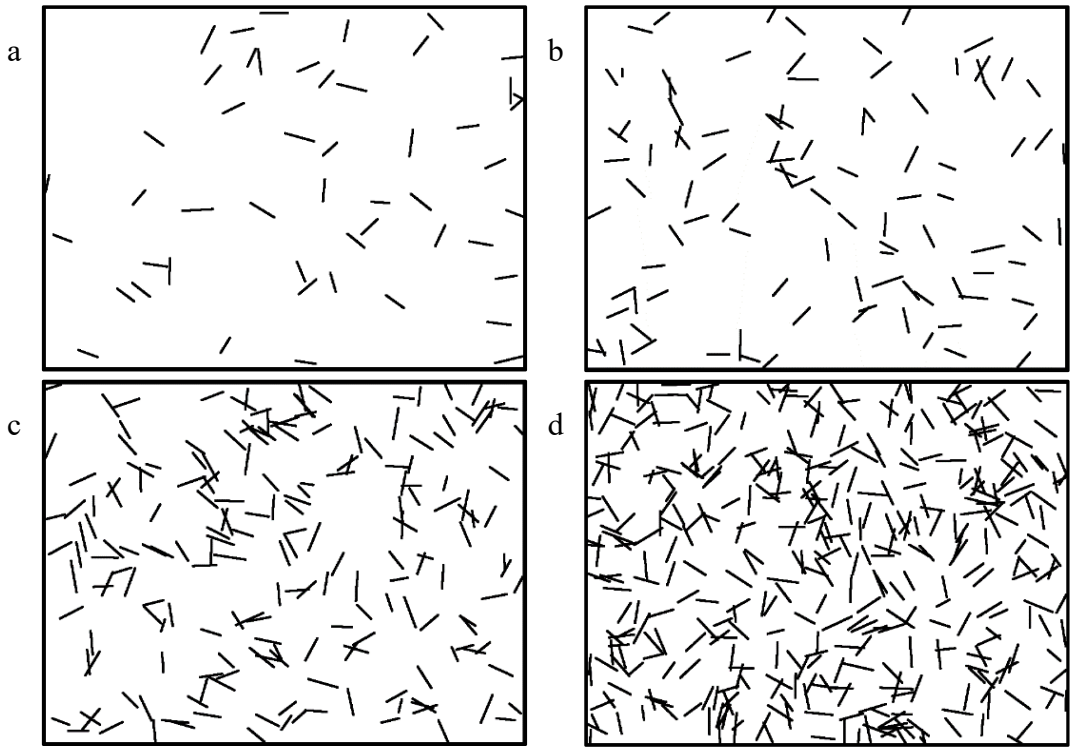

Figure 2.4: Simulated images (a) 50 fibers (b) 100 fibers (c) 200 fibers (d) 400 fibers

The simple HT method, opening method, partitioning HT method and the gradient based HT method are applied to the simulated image. Figure 2.5 shows the fiber extraction results by the simple HT method. The result for the opening method, partitioning HT and gradient based HT methods are shown in Figure 2.6, 2.7 and 2.8 respectively. Here the green line indicates the detected fiber while the yellow and red cross specifies the starting and the ending point of the line respectively.

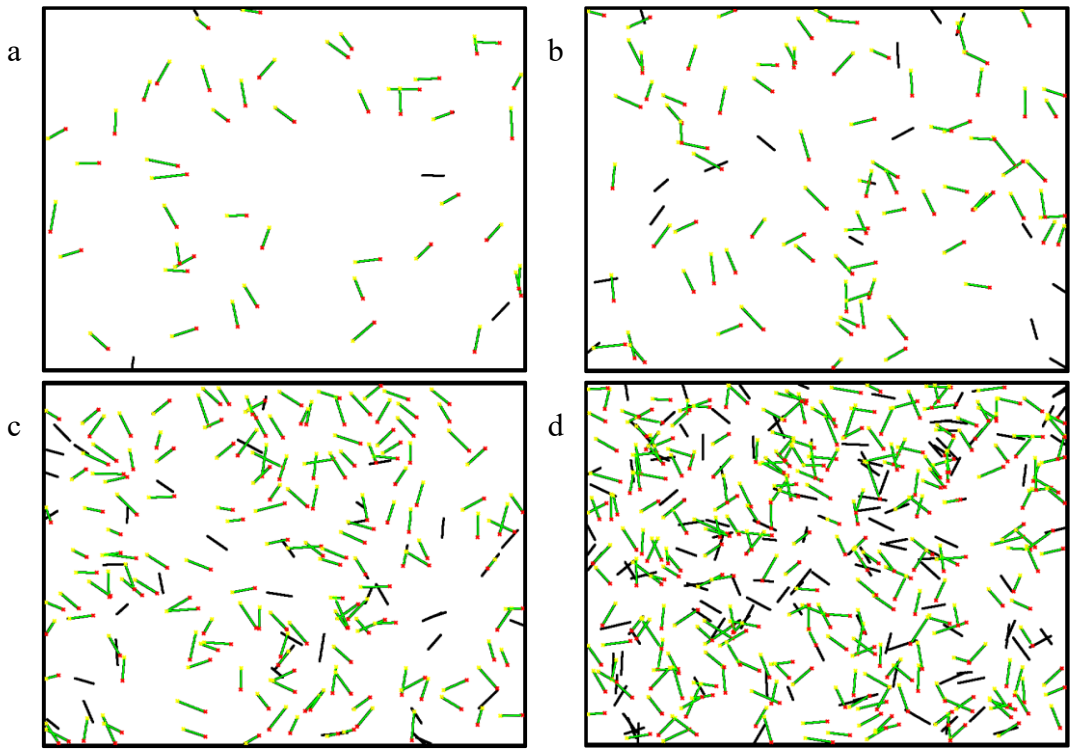

Figure 2.5: Simple HT method (a) 50 fibers (b) 100 fibers (c) 200 fibers (d) 400 fibers

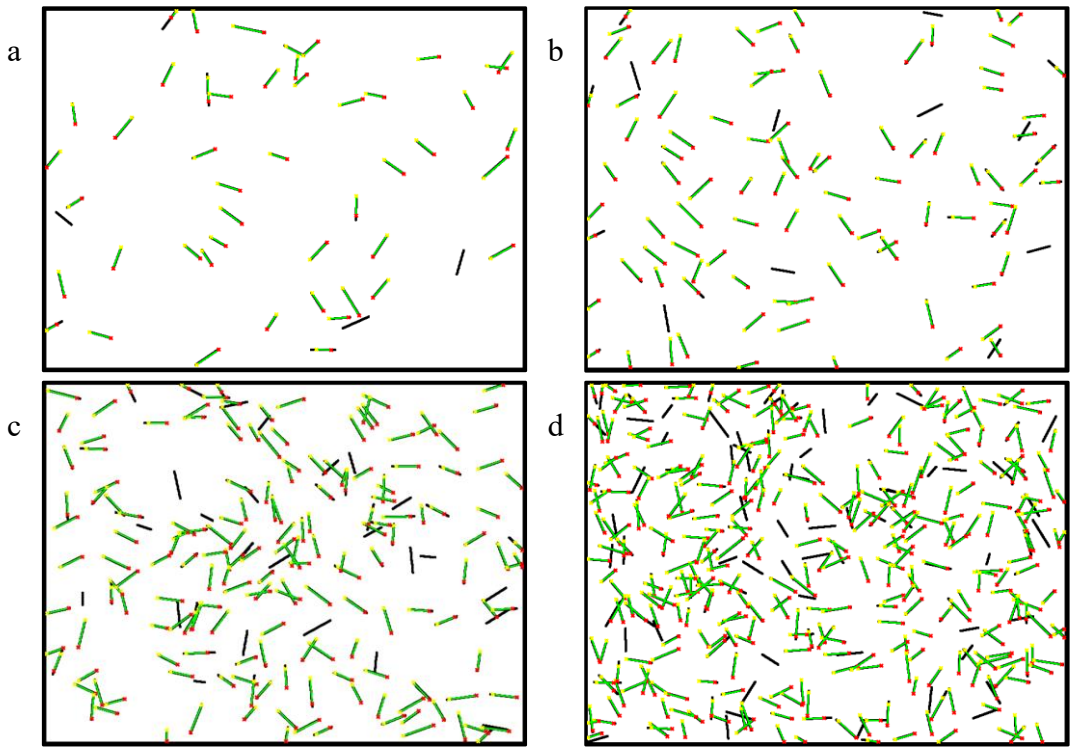

Figure: 2.6: Opening method based HT (a) 50 fibers (b) 100 fibers (c) 200 fibers (d) 400 fibers

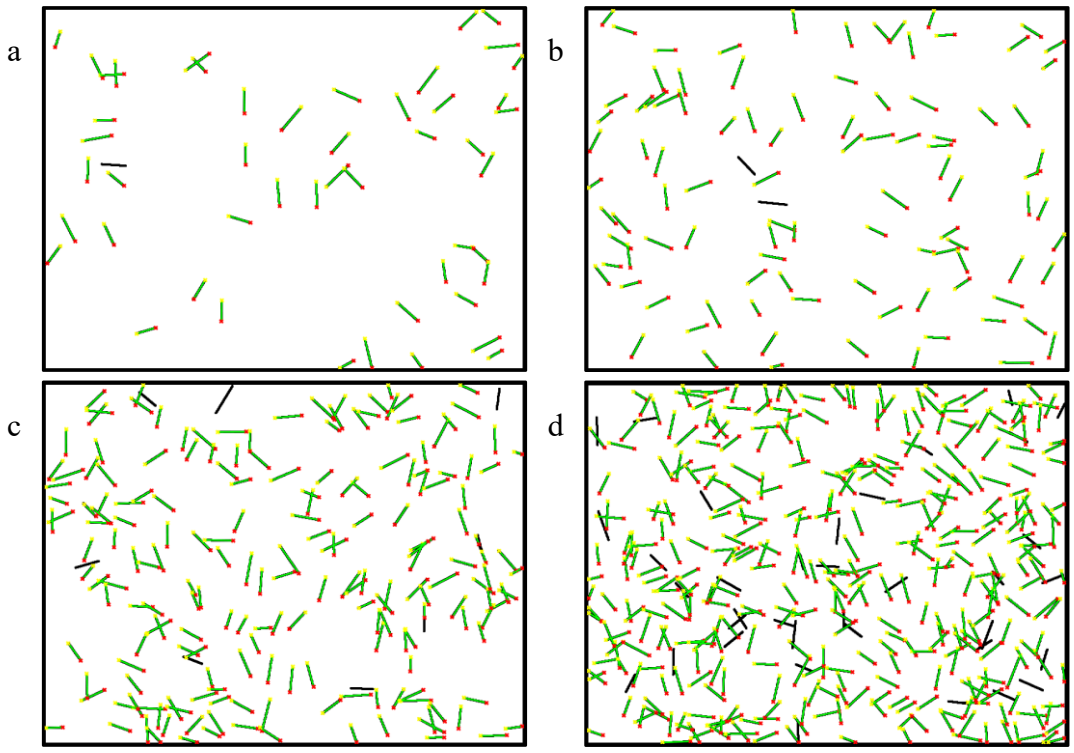

Figure 2.7: Partitioning HT (a) 50 fibers (b) 100 fibers (c) 200 fibers (d) 400 fibers

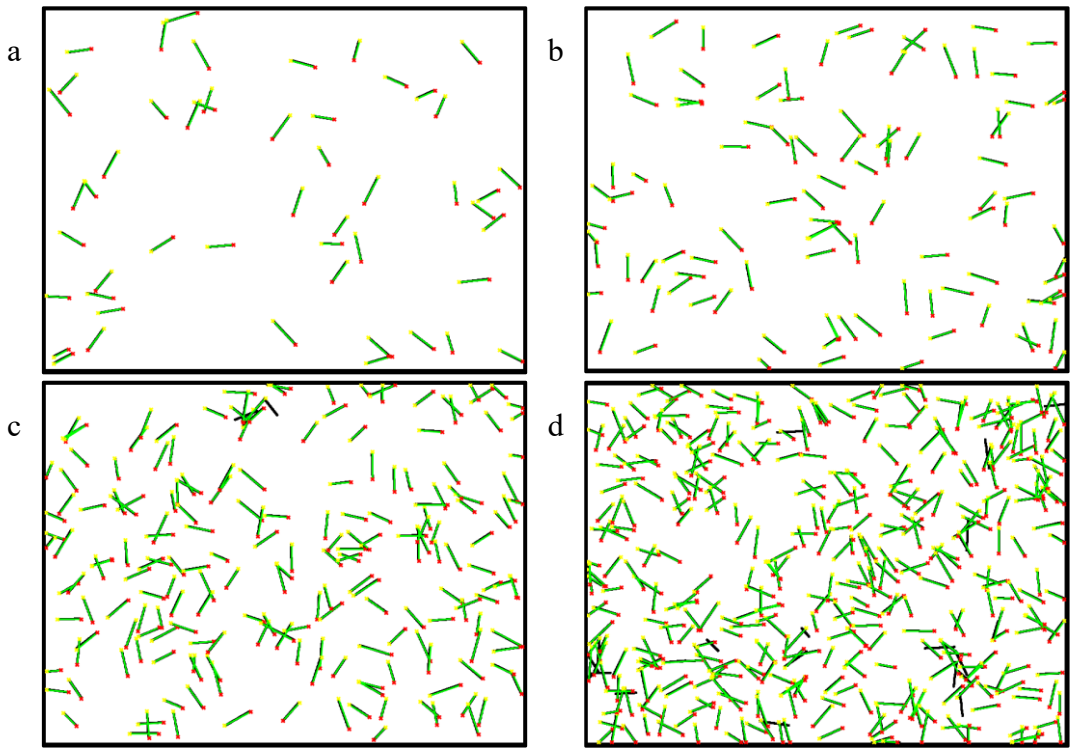

Figure 2.8: Gradient based HT (a) 50 fibers (b) 100 fibers (c) 200 fibers (d) 400 fibers

The simulation was replicated 30 times for each of the four methods with different fiber density and count the number of fibers (lines) at each run. Then by averaging the total number of fiber we get a comparative result among the methods. The result is shown in table 2.4. After analysis the result we plot an accuracy analysis result as depicted in figure 2.9.

Table 2.5: Simulation study result

Method	**No. of Fibers**	**Detected Fibers**	**Accuracy**	Maximum
Simple Hough Transform	50	46	0.92	8
	100	88	0.88	16
	200	164	0.82	45
	400	302	0.76	112
Opening Method Based Hough Transform	50	46	0.92	8
	100	90	0.90	15
	200	180	0.90	28
	400	353	0.88	61
	50	49	0.98	3

Partitioned Hough Transform	100	97	0.97	5
	200	188	0.94	19
	400	324	0.81	88
Gradient Based HT	50	50	1	0
	100	100	1	1
	200	194	0.97	8
	400	380	0.95	26

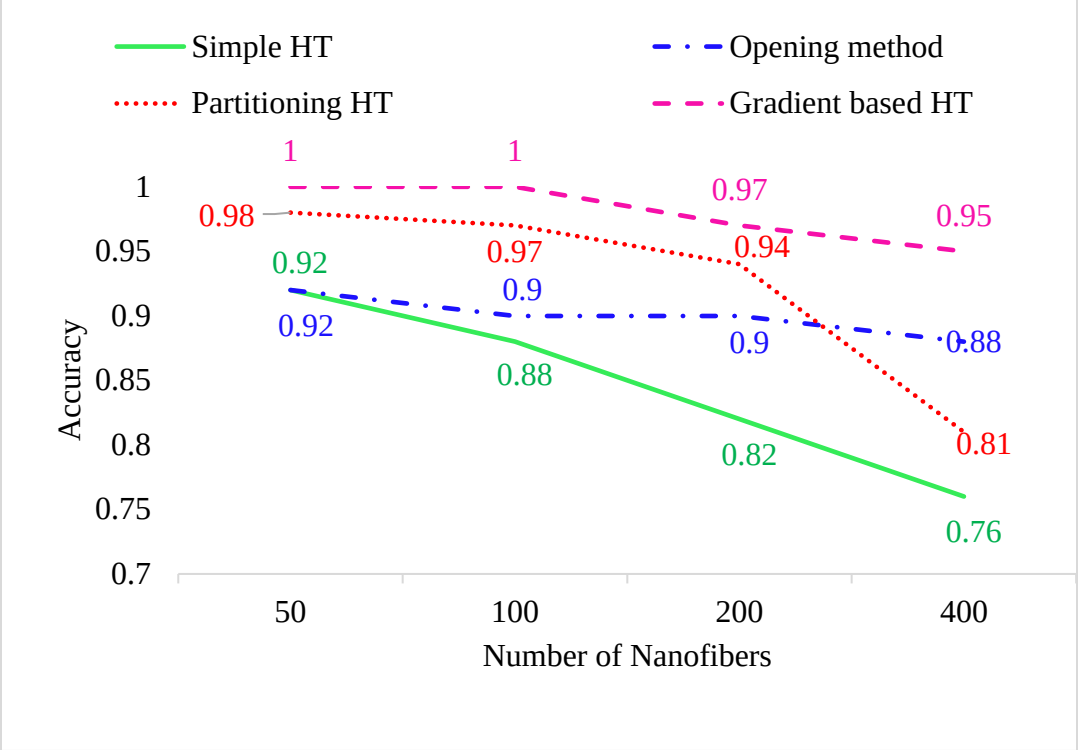

Figure 2.9: Accuracy analysis of simulation case study

Clearly, the simple HT method has the lowest extraction accuracy. It is not surprising since some pixels of other fibers on the extension of a fiber will also contribute to the cell of the accumulator that represents this fiber, which will influence the voting accuracy. In comparison, adding the partitioning step before the application of the simple HT could significantly improve the extraction accuracy. However, as the fiber density increases, the extraction accuracy for both methods decreases rapidly. The reason is that, as the fiber density increases, the useless voting by

pixels of other fibers increases, which reduces the HT based methods. If the density is too high, most of the fibers may be connected and the partitioning step is no longer working. The extreme case is that all fibers are connected. In such case the partitioning based HT would degenerate to the simple HT method. As expected, the gradient based HT method has the highest accuracy for all the four scenarios, since it could effectively eliminate the useless voting of other fibers when detecting a certain fiber. The opening method is much more stable than the other three methods in terms of the extraction accuracy. When the fiber density is lower, the accuracy of the opening method is not high. However, its advantage becomes obvious as the fiber density goes higher. Therefore, when the fiber density is extreme high, the opening method would be more preferable to all other HT based methods.

2.6 Application to real images

In this section we apply the proposed methods to extract fibers from two real images, as shown in Figure 2.10. Here the left image contains 64 fibers and the right image contains 89 fibers.

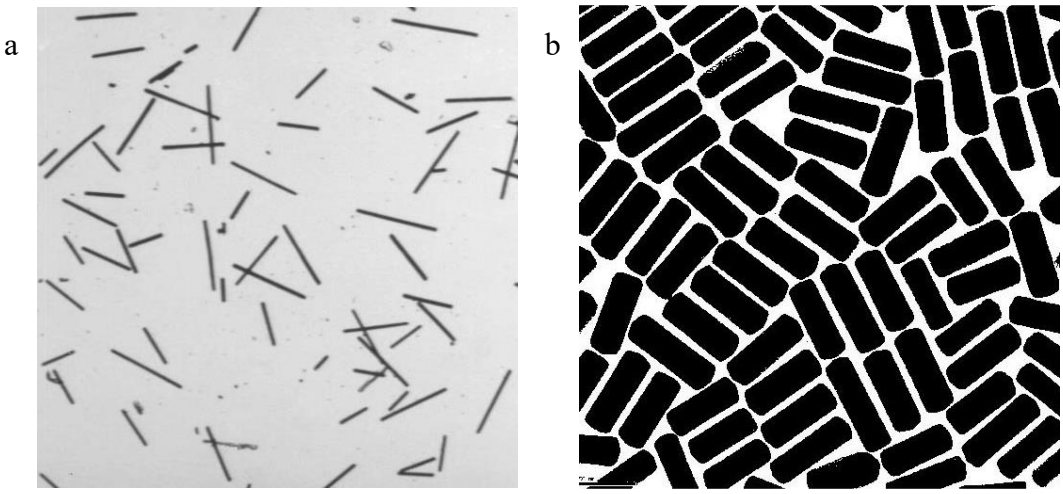

Figure 2.10: Two real images (a) 64 fibers (b) 89 fibers

Figure 2.11 shows the extraction results. The first, second, third and fourth row represent the simple HT, opening method, partitioning HT and gradient based HT respectively. Figure 2.12 shows the number of detected fibers in two images for each of the methods.

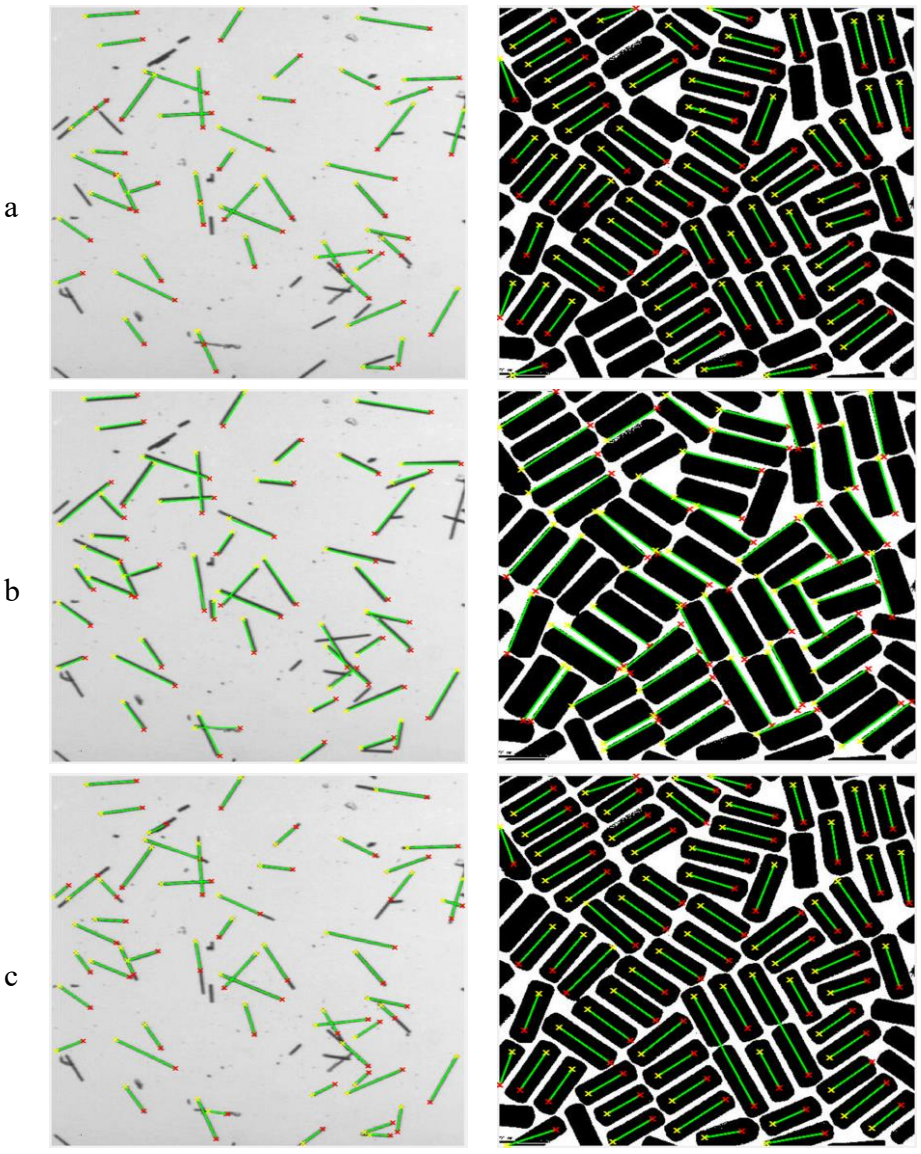

d

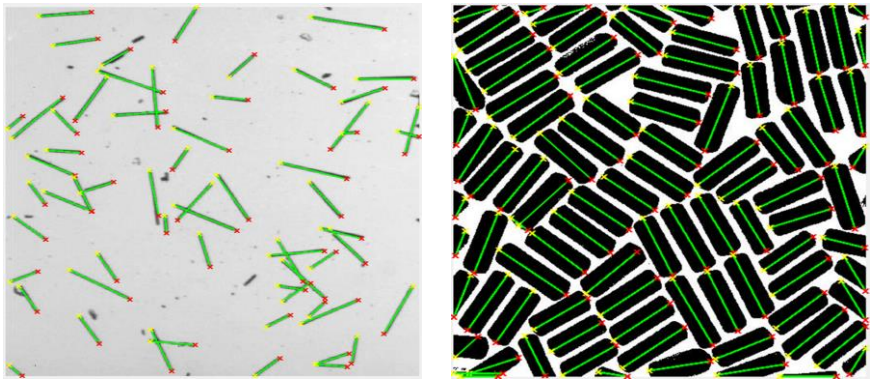

Figure 2.11: Fiber extraction from real images (a) Simple HT (b) Opening Method (c) Partitioning HT (d) Gradient HT

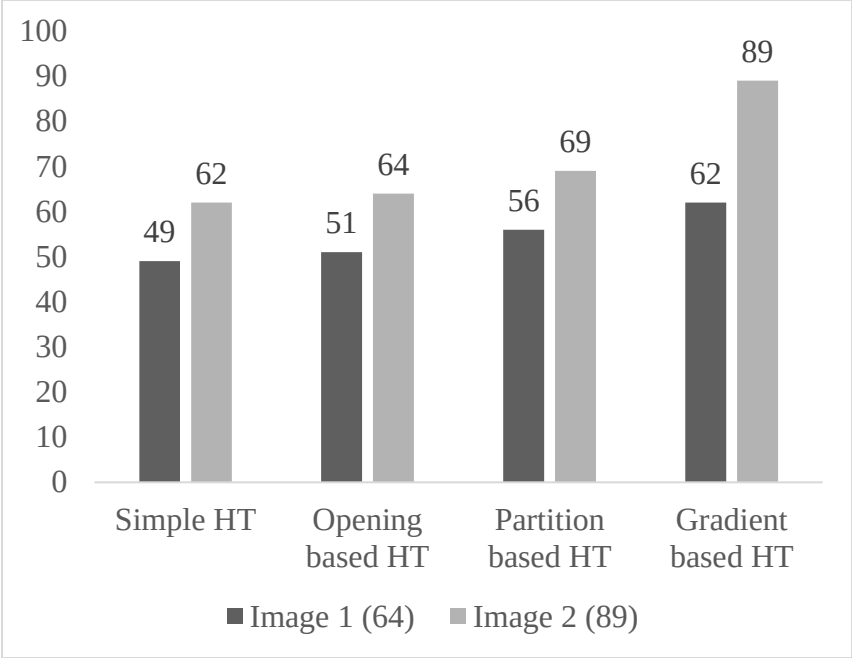

Figure 2.12: Number of detected fibers (out of 64 and 89 fibers in image 1 and image 2 respectively)

From figure 2.12, we can see that simple Hough Transform and opening method based Hough Transform performs almost with the same accuracy whereas partition based Hough

Transform outperforms than the previous two method. But it's quite obvious that gradient based Hough Transform has the highest accuracy level and this method can detect almost all the fibers in an image. If we look at figure 2.11, the first three methods fail to detect all the corner fibers. The result is zoomed and specified in figure 2.13 (a). But gradient based Hough Transfer can detect all those fibers (figure 2.13-b). Again, we can see some overlapping fibers are remained undetected in the first three methods (figure 2.13-c).

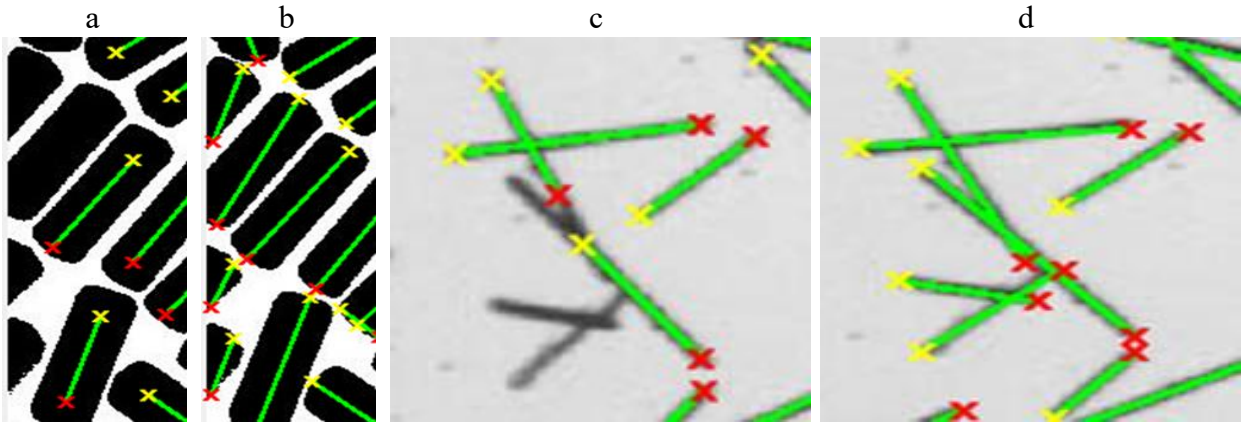

Figure 2.13: Demonstration of some undetected fibers

The reason is that, in simple Hough Transfer and partitioning Hough Transform, we use the skeleton operation before applying Hough Transfer. And as stated earlier, when there are more overlapping fibers, skeleton operation creates a very complex pattern to project a line in Hough Transform. On the other hand, in opening based method, some fibers remain undetected as we compare all the opened fibers according to the closeness of center distance and orientation, hence some fibers may be suppressed if they are close enough. This situation becomes very common when there are more overlapping fibers. The gradient based Hough Transfer method can successfully handles all the situations mentioned above. The reason is pretty obvious that as long as we can extract some gradient information form a fiber, it possible to detect that fiber by feeding that information in the Hough Transform algorithm as shown in figure 2.13 (b) and (d).

If we looked at the top left and lower middle area of image 1 in figure 16, it is noticed that some small fibers remain undetected. This may happened due to the very short length of those fibers. In the Hough Transform function, it provides a parameter called “MinLength” to give a lower limit of the length and this is a trade-off parameter. Here, we set a large value for this parameter which occurs some miss detection of relatively small fibers. A small value of this parameter causes a lot of undesired lines. The result is zoomed and depicted in figure 2.14.

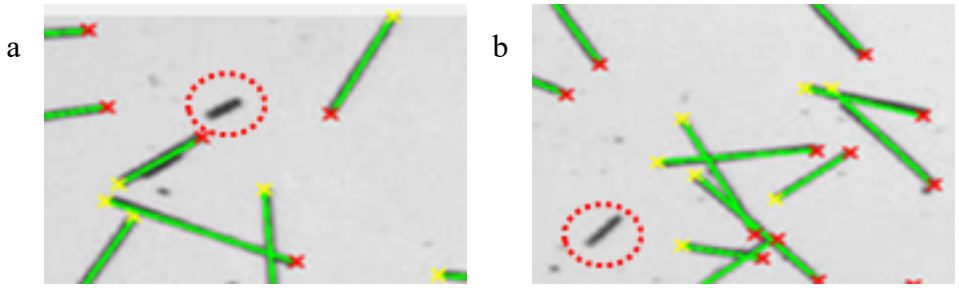

Figure 2.14: Undetected small fiber

In general, we have to trade-off among different parameters of Hough Transform namely “Threshold”, “NHoodSize”, “MinLength”, “FillGap”. Which also sometimes becomes the reason of some miss detections. It’s also noticeable that, all the methods are not identical with the nanofiber detection. Each of them have different miss detected nanofibers. This has been happened due to the implementation of different methods before the Hough Transform.

From the above discussion, we can conclude that the developed can segment the nanofibers effectively and efficiently. With the segmented fibers, the morphology analysis can be automatically extracted. But we may not forgot, there are still some problem and defects need to be focused on which could be tacked by some other methods.

Chapter 3 Nanofiber Segmentation Using DBSCAN Algorithm and extraction of morphology

In chapter 2, we described four methods to segment the fibers among which the first method is based on opening method and the rest of the three methods are based on Hough Transform algorithm. In this chapter we introduce another innovative method to segment the fibers. This method is based a well-developed data mining approach namely the density based clustering (DBSCAN) algorithm. The basic strategy is to clustering the line pixels and crossing pixels. Later we remove the crossing pixels and merge the line pixels based on their continuity and orientations.

3.1 Density Based Clustering Algorithm

DBSCAN (Density-Based Spatial Clustering of Application with Noise) is the most well-known density based clustering algorithm, first introduced in 1996 be Ester et. al. [30]. Unlike K-Means, DBSCAN does not require the number of cluster as a parameter. Rather it infers the number of clusters based on the data, and it can discover clusters of arbitrary shape. DSSCAN requires two parameter namely eps (ε – the radius of neighborhoods around a data point p) and $minPts$ (the minimum number of data points we want in a neighborhood to define a cluster). Using these two parameters, this algorithm categorizes the data points into three classes e.g. core points, border points and outliers. *Core points* are the foundation of the cluster formation. The same $eps(\varepsilon)$ is used to compute the neighborhood for each point. However, the number of points in each neighborhood may differ, which can be considered as the mass of that neighborhood. Thus the volume of the neighborhood is constant, and the mas of neighborhood is variable. So by putting the threshold on the minimum amount of mass needed to be core points, we are essentially setting a minimum density threshold. Therefore, core points are data points that satisfy a minimum density requirement. The clusters are built around the core points, so by adjusting the $minPts$ parameter, the density of clusters can be fine-tuned. A *border point* has fewer than $minPts$ within $eps(\varepsilon)$, but is in the neighborhood of a core point and *density reachable* from the core point. *Outliers* are

points that are neither *core points* nor are they close enough to a cluster to be *density-reachable* from a *core point*.

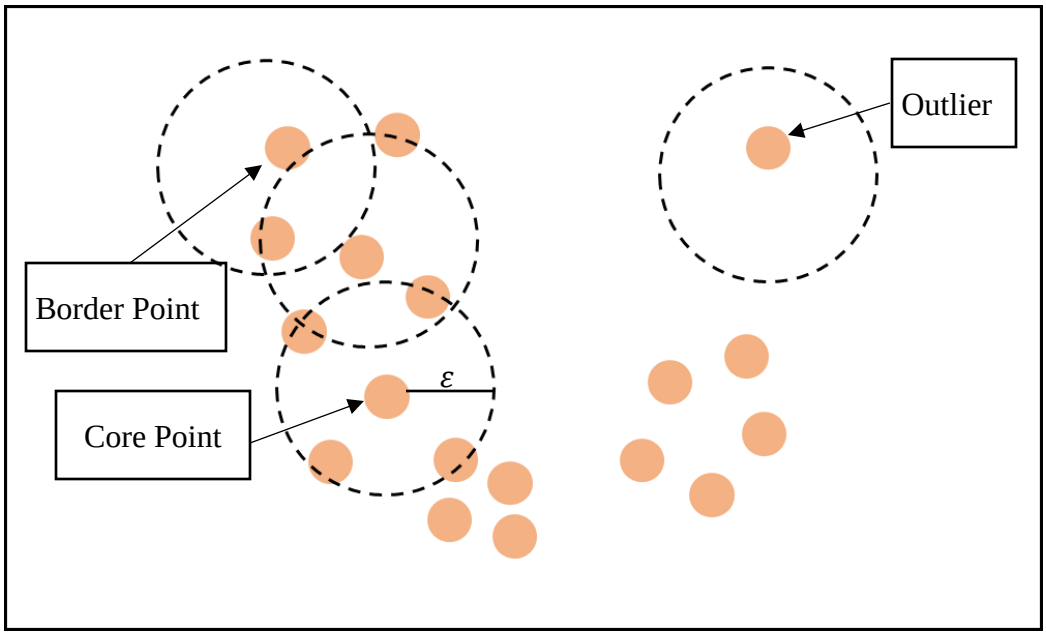

Figure 3.1: Demonstration of core point, border point and outlier with $\varepsilon = 1$ unit and $minPts = 5$

Starting from an arbitrary point, DBSCAN retrieves the number of points within the ε-neighborhood. If the points count is greater than $minPts$, a cluster is started. Otherwise, the points are considered as noise. These points might later be revisited for a different point and become a part of another cluster if it meets the required count of $minPts$ in the ε-environment. If a point found in a dense part of a cluster is also added its ε-neighborhood in this cluster. Thus, all points that are found within the ε-neighborhood are added, as is their own ε-neighborhood when they are also dense. This process is repeated until the density-connected cluster is completely found. The entire process starts again by retrieving a new unvisited point and lead to the discovery of a further cluster or noise.

3.2 Fiber Segmentation Procedure

In chapter 2, it is shown that the nanofibers in SEM images appear in tiny rectangular shape. Our intention is to detect those fibers and draw a line on each segmented fibers. Hence we used Skeletonization by the morphological thinning operation. The original structure is thinned by the use of a structuring element, e.g. a 3×3 matrix, which is convoluted over the image. This method successively erodes away pixels from the boundary until no more thinning (pixels removal) is possible. The endpoints of line segments are well preserved after thinning the image. Erosion, dilation, opening and closing are some basic morphological image operators associated with the thinning operation. See section 2.1 and the references therein for their definitions and algorithm.

Furthermore, the fibers create a complex shape by overlapping with multiple fibers. This overlapping phenomenon increases with the increase of fiber density and decreases the fiber segmentation result. To alleviate this issue, the fibers are separated using the connected component labeling algorithm [31]. This algorithm uses the binary image to generate a symbolic image in which each pixel is uniquely identified for a certain connected region based on graph traversal method. Once the first pixel of a connected component is found, all the connected component are labeled before going onto the next pixel in the image. This results in a linked list of the indexes of the pixels that are connected to each other. Using these lists of pixel indexes, separate images are created from the original image e.g. if there are n lists of connected pixels, n separate images will be generated. Each separate image may contains several fibers overlapping with each other and make the segmentation procedure complicated. This complications happens due to the crossing pixels which constitute the overlapping region shared by several fibers. To overcome this complexity our strategy is to classify the pixels as line points and crossing points and we used DBSCAN algorithm for this purpose.

By counting the number of neighboring pixels belonging to the skeleton it is possible to classify the pixels into line points and cross pints. A line point should have exactly two neighbors

whereas a cross point may have more than two neighbors. Hence, we set the DBSCAN parameters: $eps\ (\varepsilon) = 1.5$ and $minPts = 4$. It is quite a rationale that in the crossing area there will be more than 3 pixels within the ε-environment and create the cluster of every overlapping region. Rest of the pixels will be labeled as noise, which is the line points in this case as showed in figure 3.2.

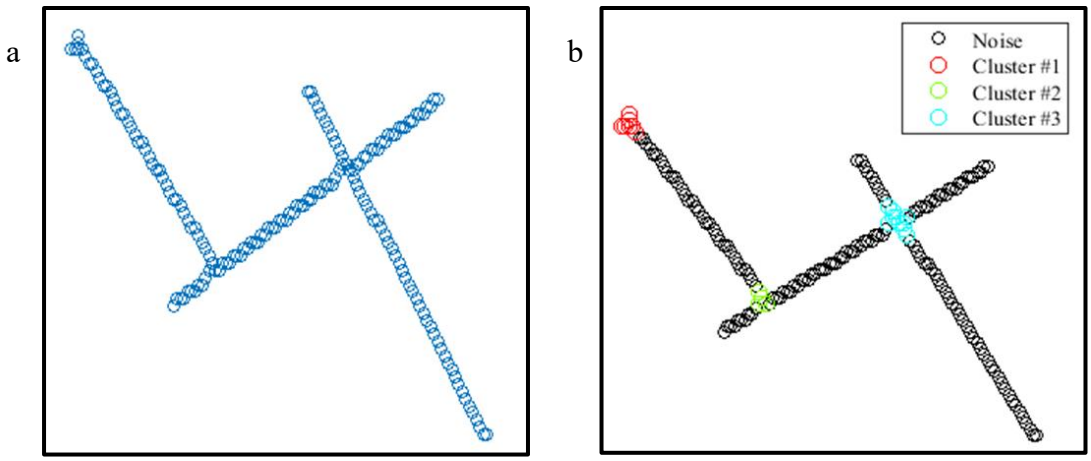

Figure 3.2: Clustering of crossing points (a) Original skeleton (b) Cluster identified at the overlapping region

Following the previous step, the crossing pixels are removed from the original set of pixels. A new dataset has been created with the noise pixels e.g. the line points. Again the DBSCAN algorithm was deployed to cluster each section of line points as shown in figure 3.3. Note that the clusters have been separated at the overlapping region. At this step, the parameters were set to $eps\ (\varepsilon) = 1.5$ and $minPts = 3$. Here, a single fiber can be separated in two or more than two clusters. Now we need to unite those clusters to get the accurate segmentation for each fiber. As the cluster can form starting from any arbitrary point, it doesn't guarantee any sequence of the clustering for a certain line i.e. fiber. Hence, the angle of the clusters was used to merge those clusters considering a certain threshold. It is based on the fact that, whatever the number of clusters a line is segmented into, their orientation should be significantly close enough. Moreover, the

center to center cluster orientation also been checked for more precise cluster merging. Following the cluster merging, the start point and the endpoints are retrieved from the merged pixels points set and drawn a line over the fiber. The algorithm is illustrated in table 3.1

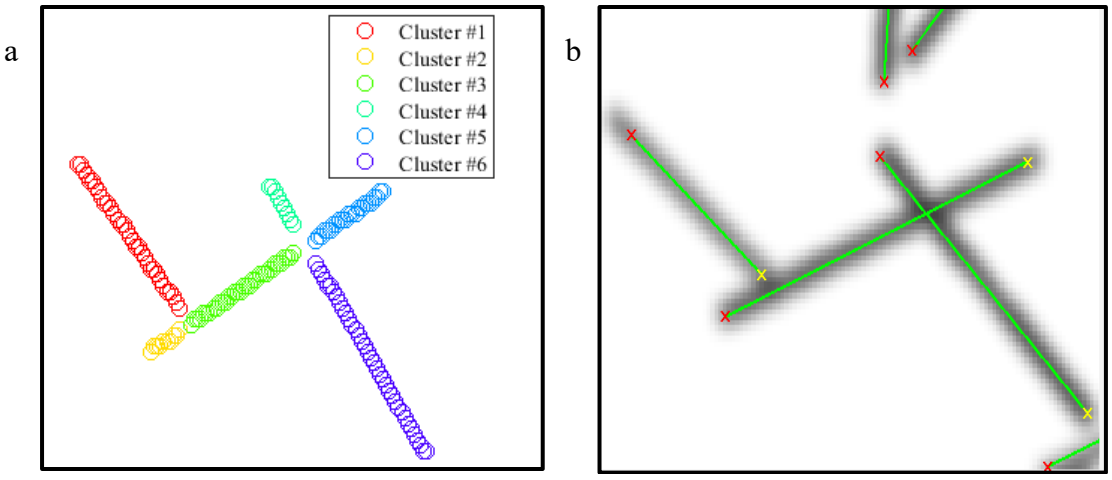

Figure 3.3: merging the line point clusters (a) lines points are cluster into different segment (b) line drawn by merging the cluster

Table 3.1: DBSCAN based fiber segmentation algorithm

1. Convert the SEM image into binary image
2. Skeletonization by morphological thinning
3. Separate the skeletonized binary image into n SEM images with each having one connected component
4. For each of the separated image
   a) Apply DBSCAN to classify the cross point
   b) Remove the cross points and create a new data set using the line points
   c) Apply DBSCAN again to cluster the line points

d) Check the continuity of cluster based on their orientation and center-to-center orientation

e) If the orientation is below a certain threshold

- Treat them as a single fiber

5. End

This proposed method is evaluated with the artificially generated SEM images. We use the same four image sets as shown in figure 2.4 in section 2.5. The four images differ in fiber density, for example, figure 2.4 (a), (b), (c) and (d) contains 50, 100, 200 and 400 fibers respectively. We deploy our method to all of these images and the extraction result is showed in figure 3.4. Here the green line indicates the segmented fiber while the yellow and red cross specify the starting and ending point respectively.

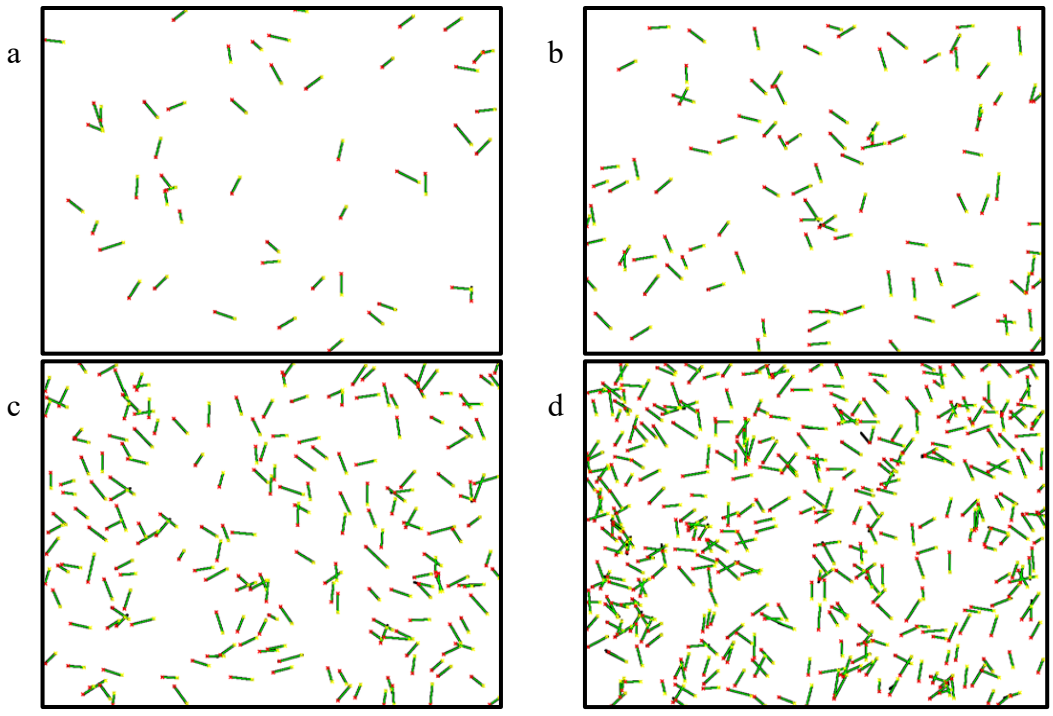

Figure 3.4: DBSCAN based fiber segmentation (a) 50 fibers (b) 100 fibers (c) 200 fibers (d) 400 fibers

The simulation was replicated 30 times. The total number of detected fibers were average across the 30 replications. Table 3.2 shows the number of detected fibers and their accuracy. It also entails the maximum number of undetected fibers (maximum error) among the 30 replications.

Table 3.2: Fiber segmentation result

Number of fibers	50	100	200	400
Detected fibers	50	100	196	389
Accuracy	1	1	0.98	0.97
Maximum error	0	0	3	16

Clearly, this method can detect all the fibers from low-density images, for example, it can detect all the fibers for 50 and 100 fibers images. While the detection accuracy slightly drops with the increase of fiber density. However, the result is still good enough for quantitative analysis. Figure 3.5 shows the fiber detection result in comparison with the Hough Transform based methods developed in chapter 2. Figure 3.6 we can see that the DBSCAN based method is more stable in terms of the maximum error.

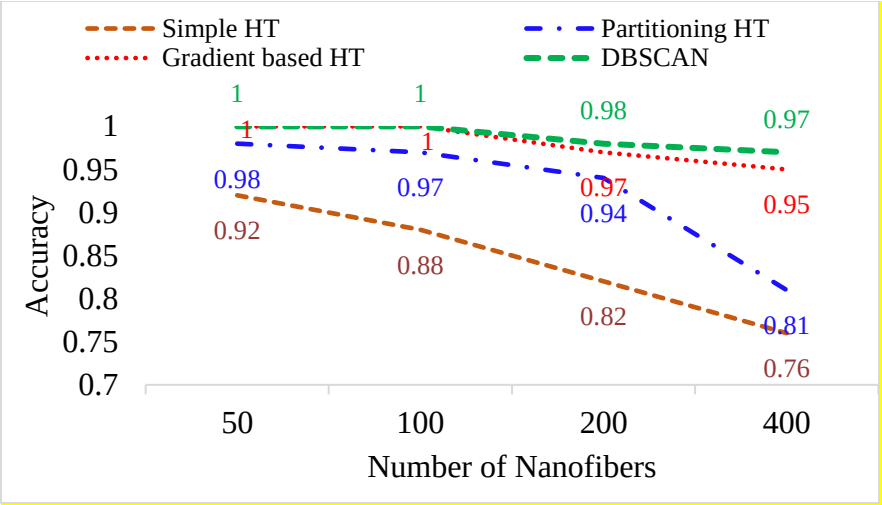

Figure 3.5: Comparison of fiber detection accuracy among HT based and DBSCAN based method

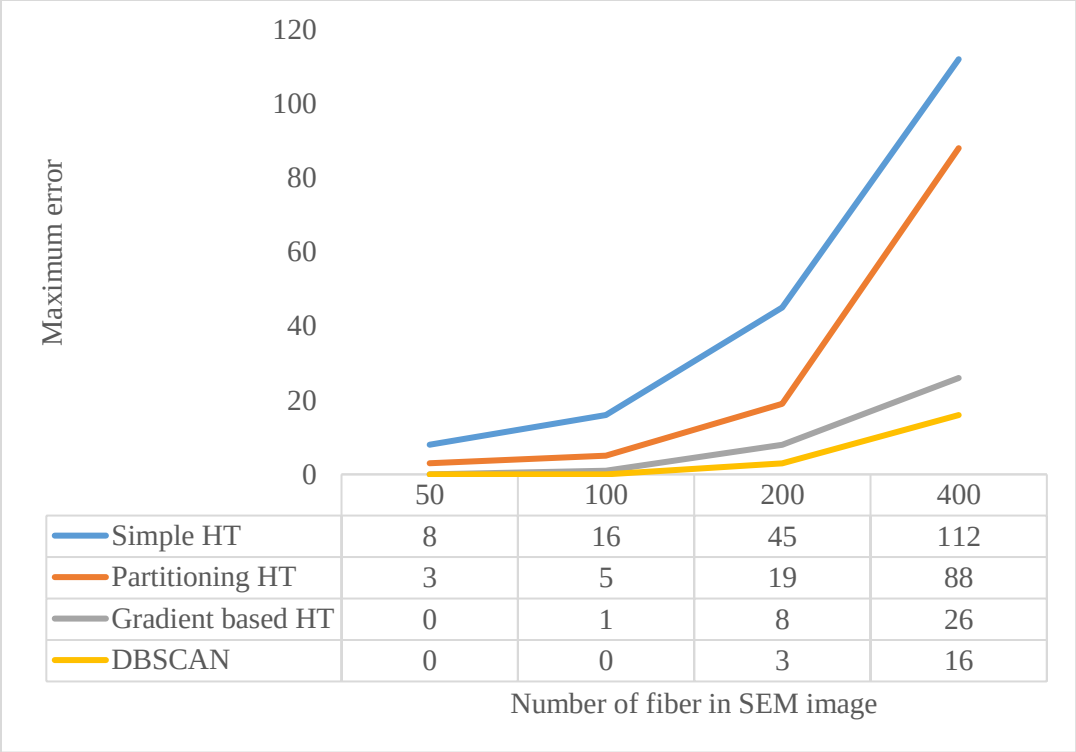

Figure 3.6: Maximum undetected fibers for different method

3.3 Morphology analysis with simulated SEM images

After segmenting the fibers, we have the spatial locations, which consist of the start coordinate $s_i(x_{si}, y_{si})$ and the end coordinate $e_i(x_{ei}, y_{ei})$, of each fibers. These coordinates are used to find the orientation (θ_i) and length (l_i) for the i^{th} fiber using equation 10 and 11.

$$\theta_i = \tan^{-1}\frac{\Delta y_i}{\Delta x_i}, where\ i = \{1,2,3, \dots \dots n\} \tag{10}$$

$$l_i = \sqrt{(x_{ei} - x_{si})^2 + (y_{ei} - y_{si})^2} \tag{11}$$

We iterate the entire procedure m times using the Monte Carlo simulation [32] to get the orientation θ_{ji} and length l_{ji} for each iteration j, where $j = \{1,2,3 \dots \dots m\}$. Later we find the $\hat{\theta}_i$ and $\hat{l}_i$ using equation 12 and finally obtain the orientation and length distribution.

$$\hat{\theta}_i = \frac{\sum_{j=1}^{m}\theta_i}{m} \text{ and } \hat{l}_i = \frac{\sum_{j=1}^{m} l_i}{m} \tag{12}$$

To test the diversity of the proposed method, six different set of orientations were used. The distribution function of the orientation is mentioned in table 3.3.

Table 3.3: Distribution function of the simulated image

Cases	Distribution function
a) Random angle (Uniform distribution)	$P_1(\theta) = \frac{1}{1800}$
b) Single Normal distribution with $\mu = 50, \sigma = 15$	$P_2(\theta) = \frac{1}{\sqrt{2\pi * 15^2}} exp\left[-\frac{(\theta - 50)^2}{2 * 15^2}\right]$
c) Single Normal distribution with $\mu = -30, \sigma = 5$	$P_3(\theta) = \frac{1}{\sqrt{2\pi * 5^2}} exp\left[-\frac{(\theta - (-30))^2}{2 * 5^2}\right]$
d) Two Normal distribution with $\mu_1 = 30, \sigma_1 = 10$ & $\mu_2 = -60, \sigma_2 = 10$	$P_4(\theta) = \frac{1}{\sqrt{2\pi * 10^2}} exp\left[-\frac{(\theta - 30)^2}{2 * 10^2}\right] + \frac{1}{\sqrt{2\pi * 10^2}} exp\left[-\frac{(\theta - (-60))^2}{2 * 10^2}\right]$
e) 3 Peaks	$P_5(\theta) = \begin{cases} \frac{1}{3}, \theta = -70 \\ \frac{1}{3}, \theta = -30 \\ \frac{1}{3}, \theta = 30 \end{cases}$
f) Single peak at $\theta = 45$	$P_6(\theta) = 1$

Six different sets of artificially SEM images were generated with all the distribution functions mentioned the above table. The simulated images are shown in figure 3.7.

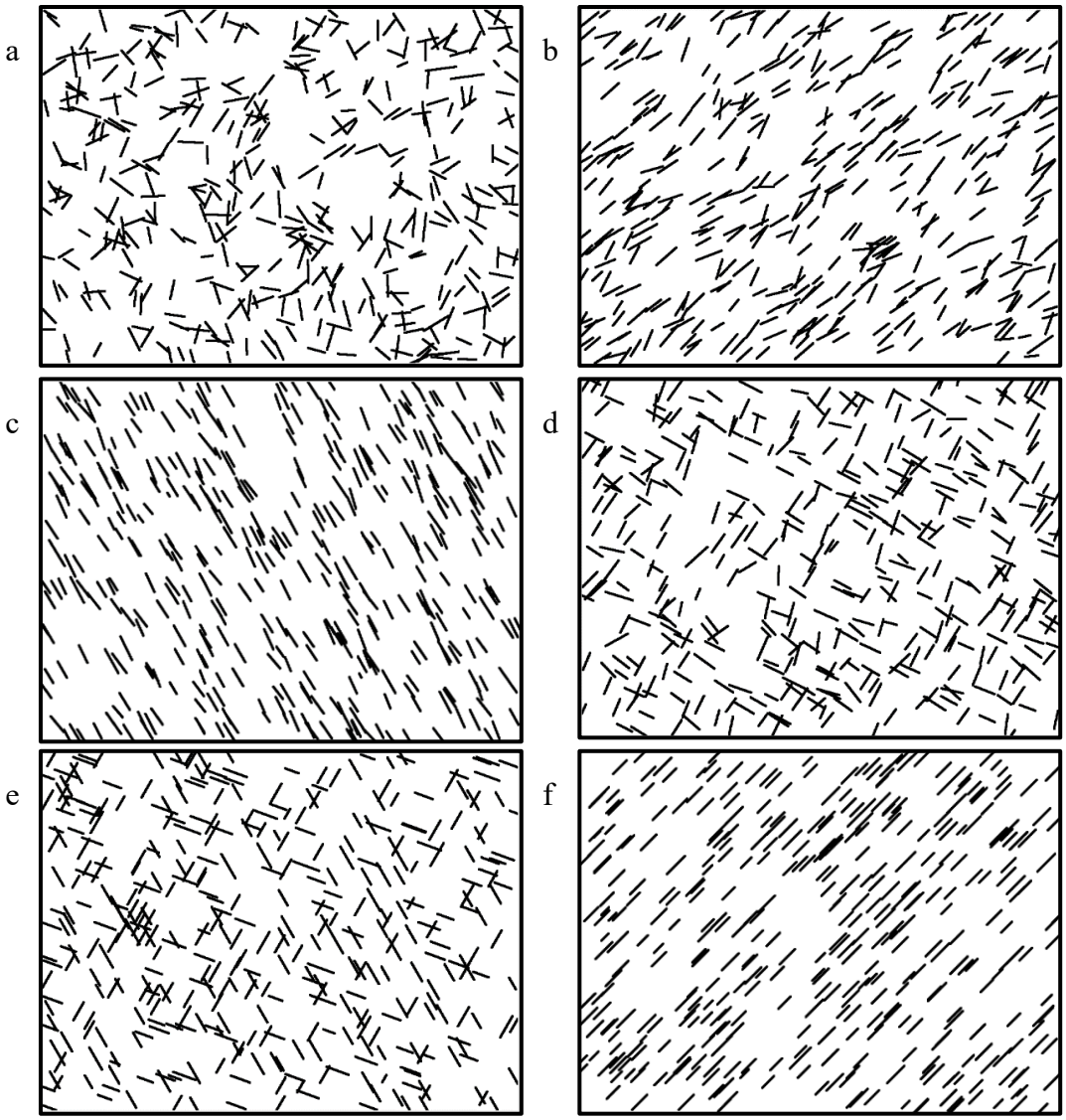

Figure 3.7: Artificial SEM images with different orientation

We apply the Monte Carlo method to obtain the empirical distribution. 30 images were generated for each of the cases to do the Monte Carlo simulation. Then the empirical distribution is compared with the true distribution. Figure 3.8 shows the result of empirical and true orientation distribution.

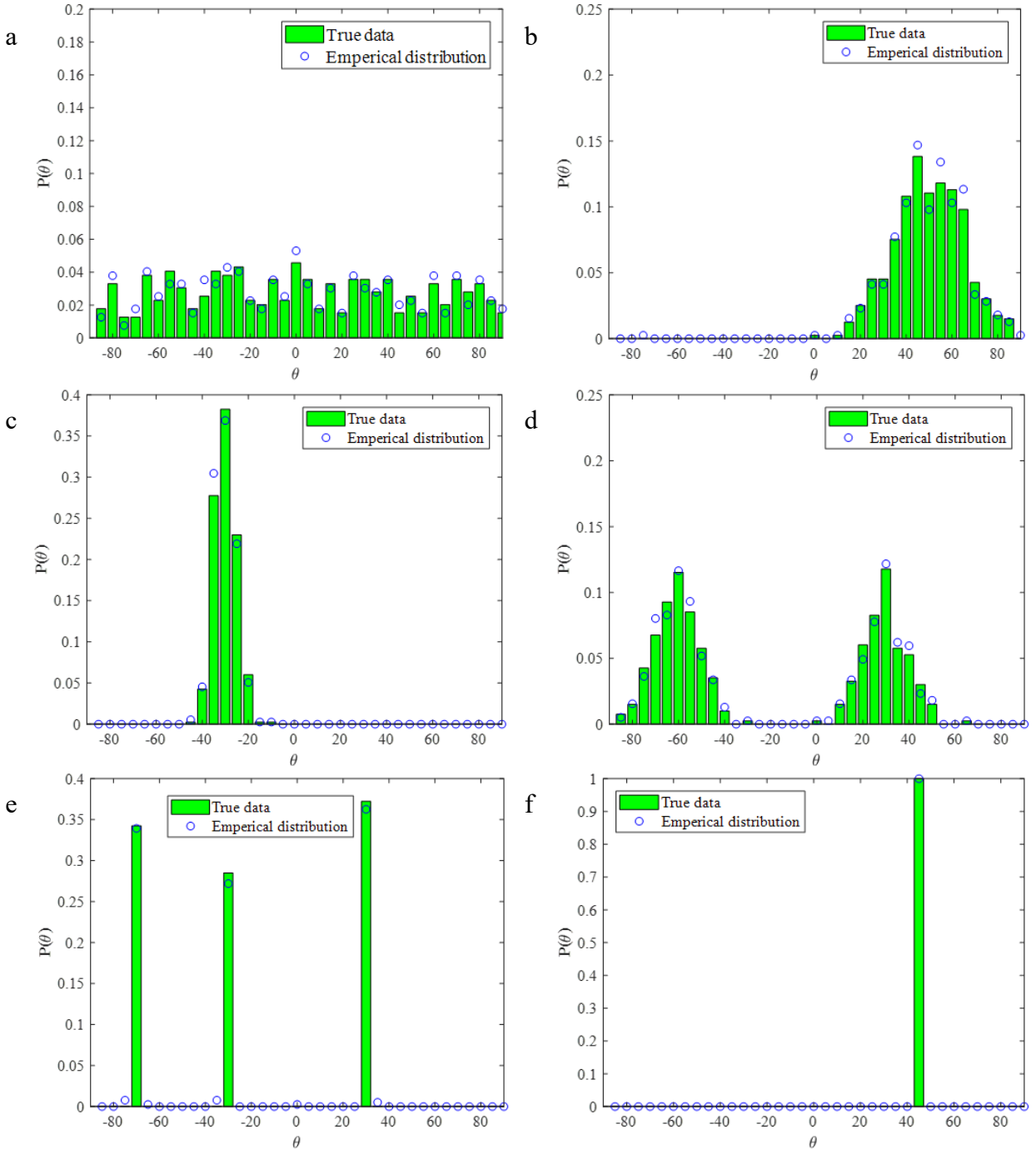

Figure 3.8: Orientation distribution of simulated images (a) uniform distribution ($\sim U(-90,90)$) (b) single normal distribution ($\sim N(50,15)$) (c) single normal distribution ($\sim N(-30,5)$) (d) Two normal distribution ($\sim N(30,10) and \sim N(-60,10)$) (e) 3 peaks at 70, -30 and 30 degrees and (f) single peak at 45 degree

Ideally, the imperial distribution should follow the similar pattern of the real distribution if it reflects the true population parameter. Among the six different distribution function, the first four function (a, b, c, and d) are continuous function and the distribution function (e and f) are desecrate function. For desecrate distribution, we can easily understand how the empirical distribution behaves in comparison to the real distribution. For continuous distribution function we use the Kolmogorov-Smirnov (K-S) test [33] to determine their goodness of fit test. . In the K-S test, the alternative hypothesis indicates that $F_n(x)$ and $F(x)$ follow different continuous distributions. The K-S statistics for a given cumulative distribution function $F(X)$ is provided by the equation 13

$$D_n = sup_x|F_n(x) - F(x)| \tag{13}$$

Where sup_x is the supremum of the set of distances and $F_n(x)$ is the empirical distribution function comes from $F(x)$. Clearly, D_n is the vertical difference between these two distribution function. If D_n is above a certain threshold we accept the alternative hypothesis and reject otherwise. The cumulative distribution functions of the empirical and true distribution are shown in figure 3.9.

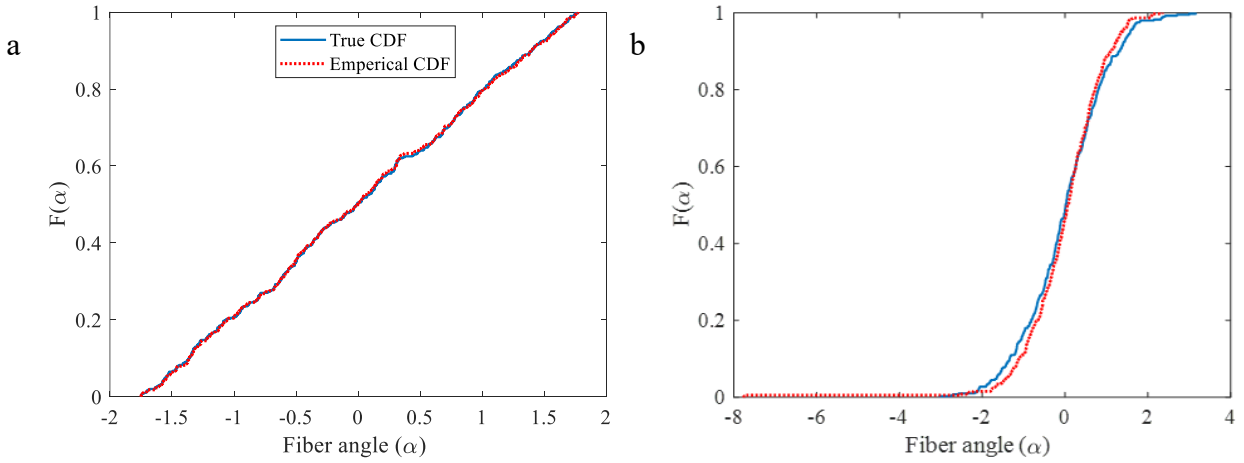

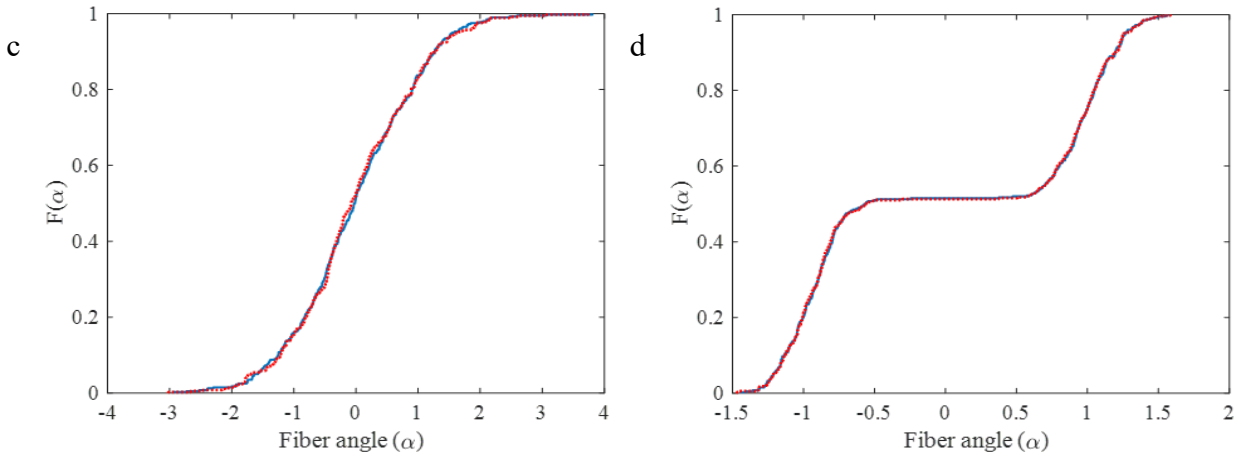

Figure 3.9: The cumulative density fuction of empirical orientation distribution in comparison with the true distribution images (a) uniform distribution ($\sim U(-90,90)$) (b) single normal distribution ($\sim N(50,15)$) (c) single normal distribution ($\sim N(-30,5)$) (d) Two normal distribution ($\sim N(30,10) and \sim N(-60,10)$)

Based on the cumulative distribution function, we get the K-S statistics result. The test statistics are 0.0365, 0.0553, 0.0717, and 0.0449 for the orientation distribution of $U(-\pi/2,\pi/2)$, $N(50,15)$, $N(-30,5)$ and $N(30,10\ and\ -60,10)$ respectively, with the corresponding p-values evaluated as 0.9992, 0.9732, 0.6762, and 0.9862 respectively. The test statistics indicates that it accept the null hypothesis for all of the four cases. In other words the empirical CDF and the true CDF are from population with the same distributions at 5% significance level. It is also obvious from figure 3.9 that all the empirical cumulative distributions are much more appropriately follow the real distribution.

We also extract the length distribution of nanofibers from the SEM images. Nano-fibers were simulated with normal distribution function with mean of 100 pixels and standard deviation of 20 pixels (see chapter 2, section 2.5 for details). As length is a scalar parameter, we do not need to test the robustness of extraction result with different orientation. Rather the accuracy of length distribution depends on the segmentation accuracy. The extracted length distribution is depicted

at figure 3.10(a) in comparison with the true distribution. We also perform the K-S test to evaluate the goodness of fit test of length distribution, as shown in figure 3.10(b).

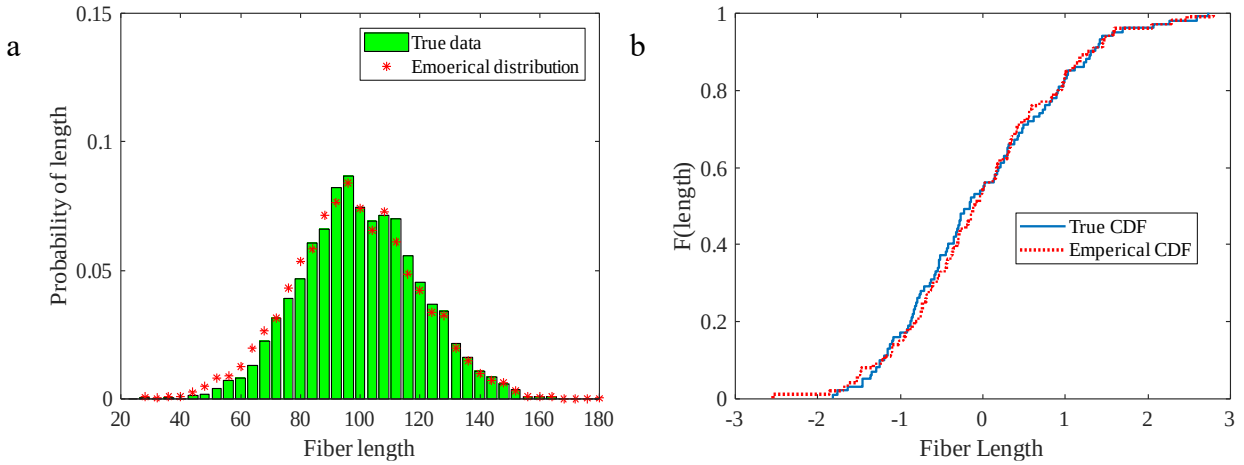

Figure 3.10: Length distribution

Form the K-S test we get the test statistic as 0.1265 and 0.1644 for low-density and high-density images respectively, with the corresponding p-value of 0.7960 and 0.2347 respectively. Again, the test statistics indicates that it doesn't reject the null hypothesis at the 5% significance level i.e. the empirical and true length distribution are from population with the same distribution. This results also reflects in figure 3.10 (a) and it is obvious that the empirical cumulative distribution closely follows the real distribution.

3.4 Application on Real Images

In this section, we apply the proposed method to perform the fiber segmentation and the morphology analysis using two real SEM images. The images are shown in 3.11. We consider 3.11(a) as the low-density image (image 1) and 3.11 (b) as the high-density image (image 2) which contains 64 and 722 (approximately) fibers respectively.

a b

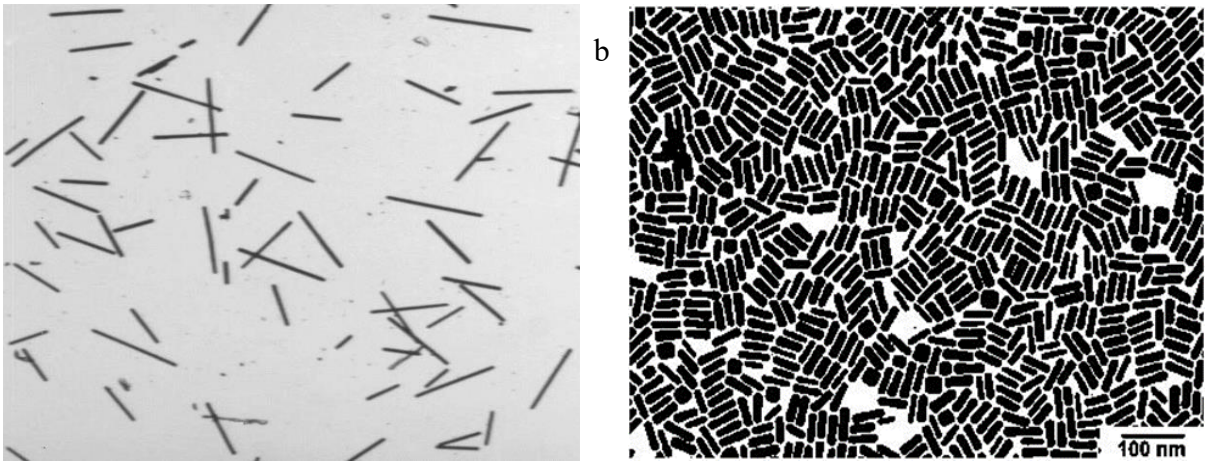

Figure 3.11: Real SEM images

The fiber segmentation result is shown in figure 3.12 (a) and 3.12 (b) respectively. From the segmentation result, we can see that our proposed method can detect al the 64 fibers for the low-density image whereas it detects 688 fibers for the very high-density image with an approximate performance of 95%. As depicted earlier, the green line indicate the detected fiber, whereas the red cross mark and the yellow cross mark specify the starting and ending point of a particular fiber.

a

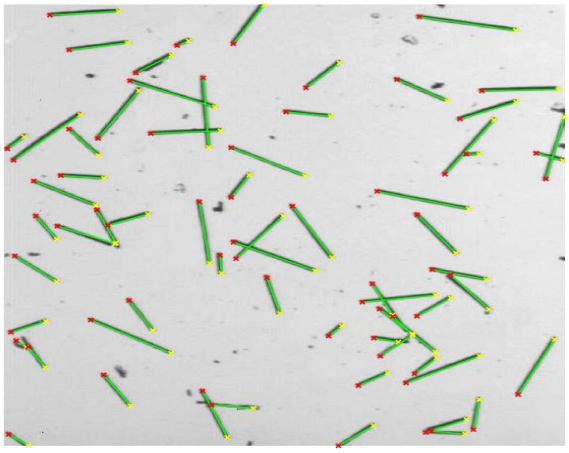

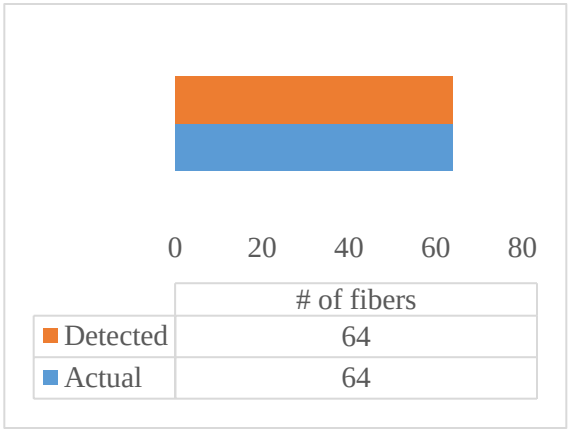

b

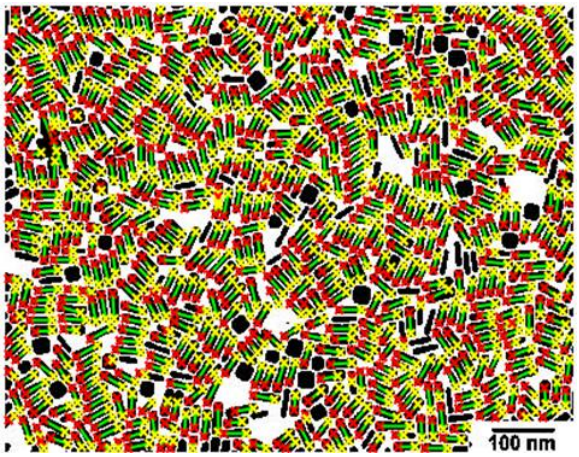

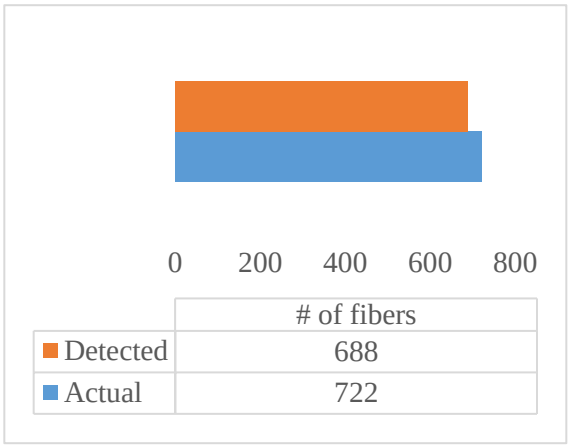

Figure 3.12: Fiber segmentation result (a) low density image (b) very high density image

Following the segmentation of fibers, we extract the orientation distribution and length distribution for both images. Figure 3.13(a) and 3.13(b) display the orientation distribution for low-density and high-density images respectively. The histogram indicates both the orientation distribution follows the uniform distribution pattern within the range of $-\pi/2$ to $\pi/2$. The length distributions for both images are shown in the figure 3.14(a) and 3.14(b) respectively.

a

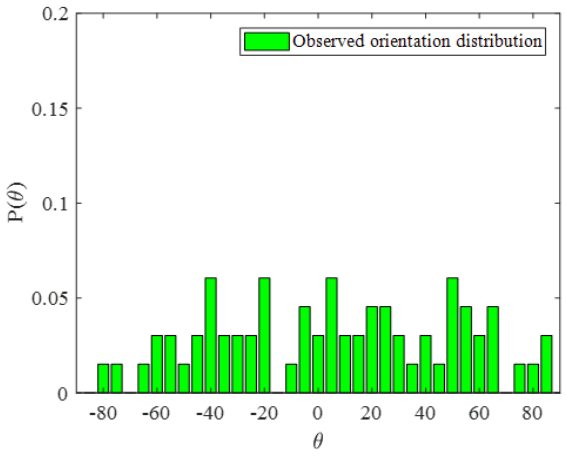

b

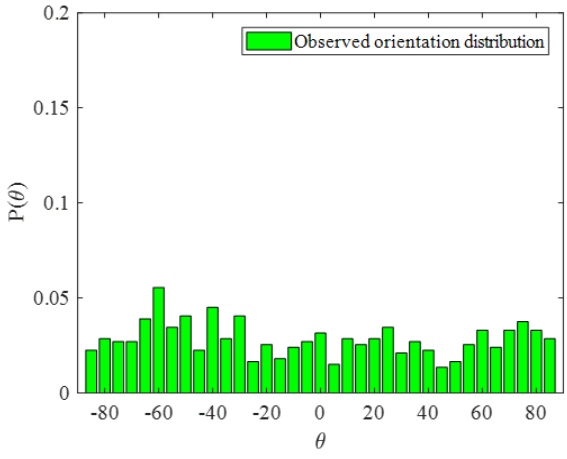

Figure 3.13: Orientation distribution (a) low-density image (b) very high density image

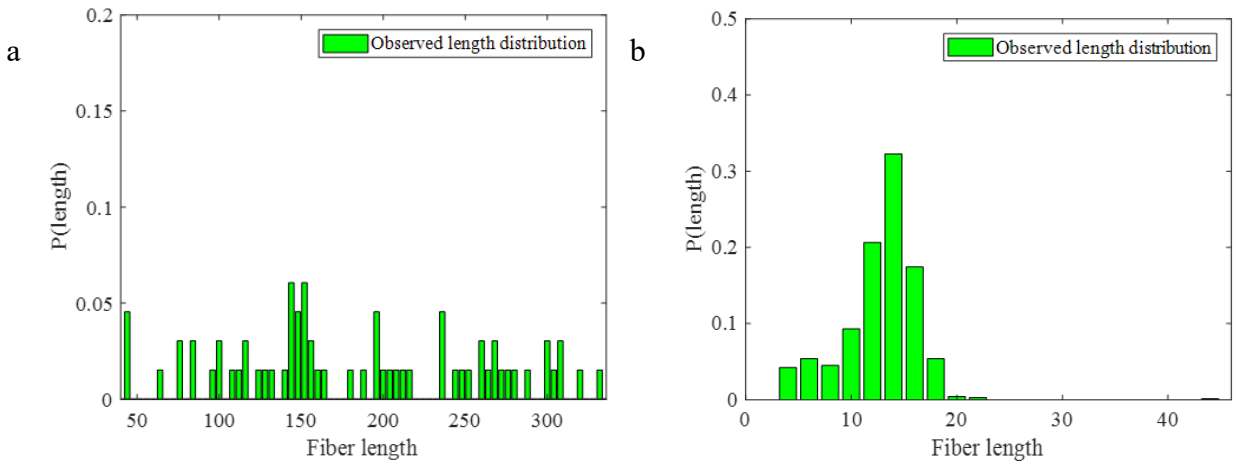

Figure 3.14: Length distribution (a) low-density image (b) very high density image

From figure 3.13 we can see that the length of fibers in image 1 (low-density image) are uniformly distributed from the minimum length of 44 pixels to the maximum length of 332 pixels. There also exits some exceptions of higher fiber density around the length of 150, 200 and 240 pixels. However the length distribution for image 2 (very high density image), approximately follow the normal distribution. It seems that the fibers length are centered on 15 pixels and remain within the boundary of 4 pixels to 23 pixels. The above fiber segmentation and the extracted orientation and length distribution provide a way to anticipate the composites properties, characteristics and functionality.

Chapter 4: Discussion and Conclusion

4.1 Research Work to Date

The current research accomplished in this thesis can be summarized as follows:

In chapter 1, we deal with the problem of extracting fibers from the SEM images of fiber reinforced composites. We proposed four different methods based on various image processing techniques, the opening method, the simple HT method, the partitioning based HT method, and the gradient based HT method. To demonstrate and compare the effectiveness of these methods, a simulation based case study has been performed using simulated SEM images with different fiber densities. The results show that the simple HT method has the worst performance. The partitioning step can improve the detection accuracy. However, its effectiveness is monotonically decreasing as the fiber density increases. The gradient based HT method has the highest detection accuracy in all four fiber density levels. The opening method is very stale and will not be affected much by the fiber density. A real case study was also conducted to illustrate the applicability of these methods.

In chapter 2, we introduce another innovatory fiber segmentation method based Density Based clustering (DBSCAN) algorithm. We also demonstrate the fiber morphology analysis in this chapter. We first segment the fibers and extract their locations by integrating some image processing operations with the DBSCAN algorithm. To demonstrate the effectiveness of this method Monte Carlo simulation was used with artificially generated SEM images varying the fibers densities. The result shows that our proposed method can extract all the fibers from the lower fiber density images. While its performance little decreases with the increase of fiber density. Nevertheless, we got up to 97% performance for the high-density images which outperforms the accuracy of the Hough Transform based methods demonstrated in chapter 1. Following the fiber segmentation, we extract the fiber orientation and length distribution. For the simulation purpose, six different orientations and their corresponding image sets have been used to justify the diversity and robustness of the extracted result. The observed distribution has been compared with the real

the distribution and using the K-S test we validate our assumed hypothesis. A real case study was also conducted to illustrate the applicability of this methods.

There are some open issues for future investigation in the fiber extraction from SEM images. First of all, the proposed methods are only applicable when the fibers are straight. However, in many fiber reinforced composites, the fibers are long in length and curved in shape. Second, due to resolution or contrast issue, the fibers may be difficult to recognize from the background of the SEM image. How to accurately extract fibers in such circumstance needs to be investigated.

4.2 Future Work

Still there are some challenges in the research of nanofiber segmentation from SEM images. In the real cases, SEM image of nanocomposites appears with more variety. The nanocomposites may have more different shapes other than the line/rectangle shapes, also, the SEM image may have several complex type, like 3D image or perspective image, these kind of the challenges require more strong/effective method to overcome the problems. With the help of machine learning and deep learning technology, it provides a wider way to find the solution we want. Therefore, in future, the goal of research work will focus on utilize the big data to build flexible intelligence artificial algorithm to fulfillment the needs. In the meanwhile, new preprocessing of the real case study will be investigated in the future time.

References

[1] Z.-M. Huang, Y.-Z. Zhang, M. Kotaki *et al.*, "A review on polymer nanofibers by electrospinning and their applications in nanocomposites," *Composites science and technology,* vol. 63, no. 15, pp. 2223-2253, 2003.

[2] https://www.zionmarketresearch.com/news/nanomaterials-market - Semtember, 2018 – "Nanomaterials Market To Report Impressive Growth, Revenue To Surge To US$16.8 Billion by 2022"

[3] E. Karden, S. Ploumen, B. Fricke *et al.*, "Energy storage devices for future hybrid electric vehicles," *Journal of Power Sources,* vol. 168, no. 1, pp. 2-11, 2007.

[4] A. Gheibi, R. Bagherzadeh, A. A. Merati *et al.*, "Electrical power generation from piezoelectric electrospun nanofibers membranes: electrospinning parameters optimization and effect of membranes thickness on output electrical voltage," *Journal of Polymer Research,* vol. 21, no. 11, pp. 1-14, 2014.

[5] D. M. Frangopol and S. Recek, "Reliability of fiber-reinforced composite laminate plates," Probabilistic Engineering Mechanics, vol. 18, pp. 119-137, 2003.

[6] V. Tomer and C. Randall, "High field dielectric properties of anisotropic polymer-ceramic composites," Journal of Applied Physics, vol. 104, p. 074106, 2008.

[7] C. Bowen, R. Newnham, and C. Randall, "Dielectric properties of dielectrophoretically assembled particulate-polymer composites," Journal of materials research, vol. 13, pp. 205-210, 1998.

[8] J. Li, L. Zhang, and S. Ducharme, "Electric energy density of dielectric nanocomposites," *Applied physics letters,* vol. 90, p. 132901, 2007.

[9] H. Tang, Y. Lin, and H. A. Sodano, "Enhanced energy storage in nanocomposite capacitors through aligned PZT nanowires by uniaxial strain assembly," Advanced Energy Materials, vol. 2, pp. 469-476, 2012.

[10] J. E. Bresenham, "Algorithm for computer control of a digital plotter," *IBM Systems journal,* vol. 4, pp. 25-30, 1965.

[11] D. Sage, F. R. Neumann, F. Hediger, S. M. Gasser, and M. Unser, "Automatic tracking of individual fluorescence particles: application to the study of chromosome dynamics," *IEEE Transactions on Image Processing,* vol. 14, pp. 1372-1383, 2005.

[12] S. Jiang, X. Zhou, T. Kirchhausen, and S. T. Wong, "Detection of molecular particles in live cells via machine learning," Cytometry Part A: The Journal of the International Society for Analytical Cytology, vol. 71, pp. 563-575, 2007.

[13] S. Kothari, Q. Chaudry, and M. D. Wang, "Automated cell counting and cluster segmentation using concavity detection and ellipse fitting techniques," in Biomedical Imaging: From Nano to Macro, 2009. ISBI'09. IEEE International Symposium on, 2009, pp. 795-798.

[14] M.-R. Jung, J.-H. Shim, B. Ko, and J.-Y. Nam, "Automatic cell segmentation and classification using morphological features and Bayesian networks," in Image Processing: Machine Vision Applications, 2008, p. 68130G.

[15] Park, Chiwoo, et al. "A multistage, semi-automated procedure for analyzing the morphology of nanoparticles." *IIE Transactions* 44.7 (2012): 507-522

[16] D. H. Ballard, "Generalizing the Hough transform to detect arbitrary shapes," Pattern recognition, vol. 13, pp. 111-122, 1981.

[17] K. Kimura, S. Kikuchi, and S.-i. Yamasaki, "Accurate root length measurement by image analysis," Plant and Soil, vol. 216, pp. 117-127, 1999.

[18] K. Kawabata, Y. Komori, T. Mishima, and H. Asama, "An asbestos fiber detection technique utilizing image processing based on dispersion color," Particulate Science and Technology, vol. 27, pp. 177-192, 2009.

[19] R. P. Heilbronner, "The autocorrelation function: an image processing tool for fabric analysis," Tectonophysics, vol. 212, pp. 351-370, 1992.

[20] Y. J. Jeon, H. W. Kang, S. H. Ko, and H. J. Sung, "Pattern analysis of aligned nanowires in a microchannel," Measurement Science and Technology, vol. 24, p. 035303, 2013.

[21] R. M. Haralick, S. R. Sternberg, and X. Zhuang, "Image analysis using mathematical morphology," IEEE transactions on pattern analysis and machine intelligence, pp. 532-550, 1987.

[22] P. V. Hough, "Method and means for recognizing complex patterns," 1962.

[23] R. O. Duda and P. E. Hart, "Use of the Hough transformation to detect lines and curves in pictures," *Communications of the ACM,* vol. 15, pp. 11-15, 1972.

[24] T. Zhang and C. Y. Suen, "A fast parallel algorithm for thinning digital patterns," Communications of the ACM, vol. 27, pp. 236-239, 1984.

[25] H. Freeman, "Computer processing of line-drawing images," ACM Computing Surveys (CSUR), vol. 6, pp. 57-97, 1974.

[26] H. Freeman and R. Shapira, "Determining the minimum-area encasing rectangle for an arbitrary closed curve," Communications of the ACM, vol. 18, pp. 409-413, 1975.

[27] E. Bribiesca and A. Guzman, "How to describe pure form and how to measure differences in shapes using shape numbers," Pattern Recognition, vol. 12, pp. 101-112, 1980.

[28] E. Bribiesca, "Arithmetic operations among shapes using shape numbers," Pattern Recognition, vol. 13, pp. 123-137, 1981.

[29] P. R. Reddy, V. Amarnadh, and M. Bhaskar, "Evaluation of stopping criterion in contour tracing algorithms," International Journal of Computer Science and Information Technologies, vol. 3, pp. 3888-3894, 2012.

[30] Ester, Martin, et al. "Density-based spatial clustering of applications with noise." *Int. Conf. Knowledge Discovery and Data Mining*. Vol. 240. 1996.

[31] Devijver, Pierre A., and C. Ronse. *Connected components in binary images: the detection problem*. John Wiley & Sons, Inc, 1984.

[32] B. J. Worton, "Using Monte Carlo simulation to evaluate kernel-based home range estimators," The Journal of wildlife management, pp. 794-800, 1995.

[33] Massey Jr, Frank J. "The Kolmogorov-Smirnov test for goodness of fit." *Journal of the American statistical Association* 46.253 (1951): 68-78.

Vita

Md. Fashiar Rahman was born on October 5, 1989 in Khulna, Bangladesh. He got his bachelor degree in Industrial & Production Engineering on spring, 2011 from Khulna University of Engineering & Technology, Bangladesh. After completing the graduation, he joined as lecturer in the department of Industrial Engineering and Management at the same university in Bangladesh. In 2017, Mr. Rahman joined in the doctoral program in Computational science at The University of Texas at El Paso.

While pursuing his degree, Mr. Rahman was appointed as a research assistant for the Department of Industrial Manufacturing and System Engineering.

Contact Information: mrahman13@miners.utep.edu